COMPARATIVE RISK ASSESSMENT OF RADIATION INDUCED SECOND CANCERS IN PATIENT WITH PROSTATE CANCER AFTER INTENSITY MODULATED RADIATION THERAPY AND STEREOTACTIC BODY RADIATION THERAPY

SAWANEE SUNTIWONG

A THESIS SUBMITTED IN PARTIAL FULFILLMENT
OF THE REQUIRMENT FOR
THE DEGREE OF MASTER OF SCIENCE
(MEDICAL PHYSICS)
FACULTY OF GRADUATE STUDIES
MAHIDOL UNIVERSITY
2016

COPYRIGHT OF MAHIDOL UNIVERSITY

Thesis
entitled

COMPARATIVE RISK ASSESSMENT OF RADIATION INDUCED SECOND CANCERS IN PATIENT WITH PROSTATE CANCER AFTER INTENSITY MODULATED RADIATION THERAPY AND STEREOTACTIC BODY RADIATION THERAPY

Sawanee Suntiwong
Miss Sawanee Suntiwong
Candidate

Assoc. Prof. Vipa Boonkitticharoen,
Ph.D. (Radiation Biology)
Major advisor

Mantana Dhanachai
Assoc. Prof. Mantana Dhanachai,
M.D., M.Sc. (Medical Epidemiology)
Co-advisor

Chomporn Sitathanee
Asst. Prof. Chomporn Sitathanee,
M.D.
Co-advisor

Prof. Patcharee Lertrit,
M.D., Ph.D. (Biochemistry)
Dean
Faculty of Graduate Studies
Mahidol University

Puangpen Tangboonduangjit
Lect. Puangpen Tangboonduangjit,
Ph.D. (Medical Radiation Physics)
Program Director
Master of Science Program in
Medical Physics
Faculty of Medicine
Ramathibodi Hospital
Mahidol University

Thesis
entitled

COMPARATIVE RISK ASSESSMENT OF RADIATION INDUCED SECOND CANCERS IN PATIENT WITH PROSTATE CANCER AFTER INTENSITY MODULATED RADIATION THERAPY AND STEREOTACTIC BODY RADIATION THERAPY

was submitted to the Faculty of Graduate Studies, Mahidol University
for the degree of Master of Science (Medical Physics)
on
May 27, 2016

Sawanee Suntiwong
.....
Miss Sawanee Suntiwong
Candidate

Mantana Dhanachai
.....
Assoc. Prof. Mantana Dhanachai,
M.D., M.Sc. (Medical Epidemiology)
Member

.....
Assoc. Prof. Kanjana Shotelersuk,
M.D.
Chair

Chomporn Sitathanee
.....
Asst. Prof. Chomporn Sitathanee,
M.D.
Member

.....
Assoc. Prof. Vipa Boonkitticharoen,
Ph.D. (Radiation Biology)
Member

.....
Prof. Patcharee Lertrit,
M.D., Ph.D. (Biochemistry)
Dean
Faculty of Graduate Studies
Mahidol University

.....
Prof. Piyamitr Sritara,
M.D., FRCPT, FACP, FRCP
Dean
Faculty of Medicine
Ramathibodi Hospital
Mahidol University

ACKNOWLEDGEMENTS

I would like to express my deepest gratitude to my major advisor, Assoc. Prof. Vipa Boonkitticharoen for her very valuable advice, guidance, supervision, encouragement, constructive comments and patience throughout this thesis. I am grateful to Assoc. Prof. Mantana Dhanachai (co-advisor), Asst. Prof. Chomporn Sitathanee (co-advisor) and Asst. Prof. Chirapha Tannanonta for their important suggestions and comments.

I would also like to thank Mrs. Pornpan Yongvithisatid, Miss Kumutinee Pairat and Mrs. Patchareporn Dechsupa for their training of the use computerized treatment planning system (MultiPlan®) and advice about the performance of CyberKnife. I would also like to show my appreciation to Miss Sukanya Rutchantuek and Miss Siwaporn Sakulsingharoj for their training of the use computerized treatment planning system (Eclipse) and the helpful advice on thermoluminescent dosimeter. My special thanks are extended to Miss Supaporn Srisuwan and Mr. Thawesak Ukamphan for their assistance with the collection of my data.

I am grateful to the division of Radiosurgery Center, Ramathibodi Hospital and the department of Therapeutic Radiology, Ramathibodi Hospital for allowing in equipment for this experiment.

I would like to thank Chulabhorn Hospital for the financial support during my medical physics programs at Mahidol University.

I wish to thank all teachers, lecturers my classmates and staffs in the School of Medical Physics, Mahidol University for their kind support throughout the entire course of study.

Finally, I am deeply grateful to my family for their financial support, entirely care, and love. The usefulness of this thesis, I dedicate to my family and all teachers who have taught me since my childhood.

Sawanee Suntiwong

COMPARATIVE RISK ASSESSMENT OF RADIATION INDUCED SECOND CANCERS IN PATIENT WITH PROSTATE CANCER AFTER INTENSITY MODULATED RADIATION THERAPY AND STEREOTACTIC BODY RADIATION THERAPY

SAWANEE SUNTIWONG 5436424 RAMP/M

M.SC. (MEDICAL PHYSICS)

THESIS ADVISORY COMMITTEE : VIPA BOONKITTICHAROEN, Ph.D., MANTANA DHANACHAI, M.D., M.Sc., CHOMPORN SITATHANEE, M.D.

ABSTRACT

This study aimed to assess the risks of second primary cancer (SPC) for prostate cancer patients treated by intensity-modulated radiation therapy (IMRT), CyberKnife stereotactic body radiation therapy (CK-SBRT) in comparing to three-dimensional conformal radiation therapy (3D-CRT). The SPC risks expressed as excess absolute risk (EAR) were determined for organs in or near the treatment fields, out-of-field and those involved in the image-guided procedures. Organ equivalent dose (OED) using a mechanistic model incorporating a dose fractionation effect, dose-volume histogram and organ-specific cancer risk parameters were employed for calculation of EAR^{org} for the primary beam component. Treatment plans for six prostate cancer patients were generated using the Eclipse treatment planning system (TPS) for both 3D-CRT and IMRT, Multiplan TPS for CK-SBRT. Ten-MV photon with 7-fields and 6-MV photon with 9-fields were delivered according to 3D-CRT plan and IMRT plan, respectively, in 39 fractions of 2 Gy; 6-MV photon with 184-289 beam orientations for CK-SBRT plan was delivered in 5 fractions of 7.25 Gy. An image-guided dose and scatter/leakage radiation for each treatment plan were measured using an Alderson radiotherapy (ART) phantom and thermoluminescent dosimeters. Associated EARs were calculated using a linear model. Ratios of OED for a certain organ site allowed a relative assessment of SPC risks (RR) between treatment modalities.

The EAR^{org} of an organ was observed as a function of organ specific carcinogenic susceptibility and OED which is dependent of the shape of dose-risk curve (bell-shaped or plateau), dose fractionation, and the organ dose-volume histogram. A hypofractionated regimen yielded a smaller area under the risk equivalent dose (RED) curve than that of conventional fractionation. Risks of SPC for all organs in or near the treatment fields of CK-SBRT were less than those from 3D-CRT and IMRT with an average RR of 0.446 ($p < 0.0001$). Comparing the dose distributions; the IMRT plan generated an RR of 0.99 for risk at the pelvic soft tissue, an inferior dose profile with a higher rectal risk (RR = 1.02, $p = 0.002$) and superior dose distribution with a lower pelvic bone sarcoma risk (RR = 0.72, $p < 0.0001$). For organs distal to the field edge, like the thyroid and brain, CK-SBRT in relation to 3D-CRT, generated an average RR of 4.46 ($p < 0.002$). Minimal patient scatter in CK-SBRT resulted in a decreasing RR from lungs (2.81) to kidneys (0.83). For IMRT, in relation to 3D-CRT, the average RR was 2.39 ($p < 0.001$). Image-guided procedures contributed much less radiation doses to organs in or near the treatment fields and also those organs receiving scatter/leakage radiation.

In conclusion, OED from the primary beam component was the major contributor of EAR^{org}, followed by scatter/leakage radiation and doses from the image-guided procedures. Overall, IMRT was associated with a highest EAR of 9.93 excess cases per 10^4 PY, 3D-CRT 8.25 per 10^4 PY and CK-SBRT 7.10 per 10^4 PY.

KEY WORDS: SECOND CANCER / RISK ASSESSMENT / ORGAN EQUIVALENT DOSE / IMRT / SBRT

82 pages

การเปรียบเทียบความเสี่ยงของการเกิดมะเร็งทุติยภูมิจากการรักษาด้วยเทคนิคการฉายรังสีแบบปรับความเข้มและรังสีรักษาร่วมพิกัดแบบทั่วร่างกายในผู้ป่วยมะเร็งต่อมลูกหมาก

COMPARATIVE RISK ASSESSMENT OF RADIATION INDUCED SECOND CANCERS IN PATIENT WITH PROSTATE CANCER AFTER INTENSITY MODULATED RADIATION THERAPY AND STEREOTACTIC BODY RADIATION THERAPY

SAWANEE SUNTIWONG 5436424 RAMP/M

วท.ม. (ฟิสิกส์การแพทย์)

คณะกรรมการที่ปรึกษาวิทยานิพนธ์ : วิภา บุญกิตติเจริญ, Ph.D., มัณฑนา ธนะไชย, M.D., M.Sc., ชมพร สีตะธนี, M.D.

บทคัดย่อ

งานวิจัยนี้มีวัตถุประสงค์เพื่อเปรียบเทียบความเสี่ยงของการเกิดมะเร็งทุติยภูมิในผู้ป่วยมะเร็งต่อมลูกหมากด้วยเทคนิคการฉายรังสีแบบปรับความเข้ม (IMRT) หรือรังสีรักษาร่วมพิกัดแบบทั่วร่างกายด้วยเครื่อง CyberKnife (CK-SBRT) กับเทคนิคการฉายรังสีแบบสามมิติ (3D-CRT) งานวิจัยนี้จะประเมินค่าความเสี่ยงด้วยค่า excess absolute risk (EAR) สำหรับอวัยวะที่อยู่ภายในหรือใกล้เคียงกับลำรังสี อวัยวะที่ได้รับรังสีเอกซ์เพื่อตรวจสอบหรือนำวิถีลำรังสีรักษา ตลอดจนอวัยวะอยู่นอกลำรังสีรักษา EAR จากรังสีปฐมภูมิคำนวณจากค่า OED ที่รวมผลของ dose fractionation dose distribution และค่าความไวของการเกิดมะเร็งจำเพาะต่ออวัยวะที่ศึกษา ใช้ข้อมูลจากผู้ป่วยมะเร็งจำนวน 6 ราย ในการวางแผนการรักษาทั้ง 3 เทคนิค 3D-CRT ใช้พลังงาน 10 MV มีทิศทางการเข้าลำรังสี 7 ทิศทาง IMRT ใช้พลังงาน 6 MV มีทิศทางการเข้า 9 ทิศทาง และเทคนิค CK-SBRT ใช้พลังงาน 6 MV ทิศทางการเข้าลำรังสีเฉลี่ย 184–289 3D-CRT และ IMRT จะให้รังสีปริมาณ 2 Gy จำนวน 39 ครั้ง และ CK-SBRT ให้รังสีขนาด 7.25 Gy จำนวน 5 ครั้ง สำหรับปริมาณรังสีเอกซ์เพื่อตรวจสอบหรือนำวิถี และปริมาณรังสีกระเจิงหรือรั่วไหลจะวัดในหุ่นจำลองโดยใช้ thermoluminescent dosimeter (TLD) ค่า EAR จะคำนวณจากสมการ OED เส้นตรง ความเสี่ยงสัมพัทธ์ (relative risk; RR) ระหว่างแผนการรักษาที่แตกต่างจะคำนวณจากอัตราส่วนของ OED ของแผนการรักษาเหล่านี้

EAR ของอวัยวะที่ศึกษาจะขึ้นกับค่าของ OED ซึ่งถูกกำหนดโดย dose-fractionation และ dose distribution OED จากการฉายรังสีแบบ hypofractionation จะมีค่าน้อยกว่าการฉายแบบ conventional fractionation การเสี่ยงต่อการเกิดมะเร็งทุติยภูมิในอวัยวะที่อยู่ในหรือใกล้ลำรังสีจากเทคนิค CK-SBRT มีอัตราต่ำกว่า 3D-CRT หรือ IMRT โดยมีค่า RR เฉลี่ย = 0.446 ($p < 0.0001$) เทคนิค IMRT เมื่อเทียบกับ 3D-CRT เนื้อเยื่ออุ้งเชิงกรานมีค่า RR = 0.99 เพราะการกระจายตัวของรังสีที่เหมือนกัน RR ของลำไส้ตรงมีค่า 1.02 ($p = 0.002$) เนื่องจากการกระจายตัวของรังสีที่ด้อยกว่า ในขณะที่ RR ของกระดูกในอุ้งเชิงกราน มีค่า 0.72 ($p < 0.0001$) เพราะการกระจายตัวของรังสีที่ดีกว่า สำหรับอวัยวะที่อยู่ห่างจากลำรังสีเช่น ต่อมธัยรอยด์และสมอง CK-SBRT มีค่าความเสี่ยงมากกว่า 3D-CRT (RR = 4.46, $p < 0.0002$) แต่ CK-SBRT ก่อให้เกิดรังสีกระเจิงในผู้ป่วยน้อยกว่า 3D-CRT ค่า RR ของอวัยวะที่อยู่ใกล้จะมีค่า RR ลดลง เช่น ปอด (RR = 2.81) และไต (RR = 0.83) สำหรับเทคนิค IMRT เมื่อเทียบกับ 3D-CRT จะมีค่า RR เฉลี่ยคือ 2.39 ($p < 0.0001$) ปริมาณรังสีเอกซ์เพื่อการตรวจสอบหรือนำวิถีลำรังสีรักษาเพิ่มความเสี่ยงต่อการเกิดมะเร็งทุติยภูมิเพียงเล็กน้อย

ผลการวิจัยนี้มีข้อสรุปคือ รังสีปฐมภูมิมีผลต่อการเสี่ยงการเกิดมะเร็งทุติยภูมิมากที่สุด ตามด้วยรังสีกระเจิงหรือรั่วไหล และรังสีเอกซ์เพื่อตรวจสอบหรือนำวิถี โดยรวบยอด EAR จาก IMRT มีค่าสูงสุดคือ 9.93 ต่อ 10^4 PY รองลงมาคือ 3D-CRT มีค่า 8.25 ต่อ 10^4 PY และน้อยที่สุดคือ CK-SBRT มีค่า 7.10 ต่อ 10^4 PY

82 หน้า

CONTENTS

		Page
ACKNOWLEDGEMENTS		**iii**
ABSTRACT (ENGLISH)		**iv**
ABSTRACT (THAI)		**v**
LIST OF TABLES		**vii**
LIST OF FIGURES		**ix**
LIST OF ABBREVIATION		**xii**
CHAPTER I	**INTRODUCTION**	**1**
CHAPTER II	**OBJECTIVES**	**7**
CHAPTER III	**LITERATURE REVIEWS**	**9**
CHAPTER IV	**MATERIALS AND METHODS**	**18**
CHAPTER V	**RESULTS**	**35**
CHAPTER VI	**DISCUSSIONS**	**58**
CHAPTER VII	**CONCLUSIONS**	**63**
REFERENCES		**65**
APPENDIX		**71**
BIOGRAPHY		**82**

LIST OF TABLE

Table		Page
4.1	The 3D-CRT planning data for six prostate cancer patients	19
4.2	The IMRT planning data for six prostate cancer patients	19
4.3	The CK-SBRT planning data for six prostate cancer patients	20
4.4	Preheat and annealing parameters for TLD-700 rods and TLD-100H chips	24
4.5	Parameters for RED and EAR calculations	29
4.6	Nine locations of TLD in ART phantom for scatter/leakage dose measurement	30
4.7	Parameters for EAR calculations for organs in out-of-field regions	31
4.8	Image-guided protocols and phantom measurement dose measurement.	32
4.9	Points of imaging dose measurement in ART phantom	33
5.1	RED curve inflection points and doses at different volume peaks from differential dose-volume histograms	41
5.2	OEDs and EARs for organs in-field and near-field of treatment	43
5.3	Scatter/leakage doses from TLDs measurement outside treatment fields for 3D-CRT, IMRT and CK-SBRT	45
5.4	Scatter/leakage doses and EARs for organs in out-of-field	47
5.5	Imaging doses from the image-guided protocol used in 3D-CRT	49
5.6	Imaging doses from the image-guided protocol used in IMRT	50
5.7	Imaging doses from the image-guided protocol used in CK-SBRT	51
5.8	EARs for organs receiving doses from image-guided procedures used in 3D-CRT, IMRT and CK-SBRT	53
5.9	EARs for 3D-CRT from primary beam component, scatter/leakage radiation and image-guided procedures	54

LIST OF TABLES (cont.)

Table		Page
5.10	EARs for IMRT from primary beam component, scatter/leakage radiation and image-guided procedures	55
5.11	EARs for CK-SBRT from primary beam component, scatter/leakage radiation and image-guided procedures	55
5.12	EAR_{total} for 3D-CRT, IMRT and CK-SBRT	56
A.1	The element correction coefficient (ECC_i) of 100 TLDs	74
A.2	The individual sensitivity factor (k_{si}) of TLD-100H	79

LIST OF FIGURES

Figure		Page
3.1	The linear dose-response relationship	11
3.2	The linear-exponential dose-response relationship	12
3.3	The linear-plateau dose-response relationship for breast, bladder and stomach cancer	13
4.1	Clinac iX linear accelerator	21
4.2	Accuray CyberKnife G4 System	22
4.3	Thermoluminescence dosimeter type 700 rods in planchet	23
4.4	Thermoluminescence dosimeter type 100H chips in planchet	24
4.5	Thermoluminescence dosimeter reader	25
4.6	Thermoluminescence annealing oven	25
4.7	The Female Alderson Radiation Therapy Phantom	26
4.8	Position of TLDs in ART phantom for scatter/leakage dose measurement	31
4.9	TLD positions for imaging dose measurement of 3D-CRT, IMRT	33
5.1	(A): Risk-equivalent dose (RED) curves for in-field pelvic soft tissue from 3D-CRT, IMRT and CK-SBRT (B): Differential dose-volume histogram for in-field pelvic soft tissue from 3D-CRT, IMRT and CK-SBRT (C): Volume weighted RED curves for in-field pelvic soft tissue from 3D-CRT, IMRT and CK-SBRT	36

LIST OF FIGURES (cont.)

Figure		Page
5.2		37
	(A): Risk-equivalent dose (RED) curves for near-field pelvic soft tissue from 3D-CRT, IMRT and CK-SBRT	
	(B): Differential dose-volume histogram for near-field pelvic soft tissue from 3D-CRT, IMRT and CK-SBRT	
	(C): Volume weighted RED curves for near-field pelvic soft tissue from 3D-CRT, IMRT and CK-SBRT	
5.3		38
	(A): Risk-equivalent dose (RED) curves for pelvic bone from 3D-CRT, IMRT and CK-SBRT	
	(B): Differential dose-volume histogram for pelvic bone from 3D-CRT, IMRT and CK-SBRT	
	(C): Volume weighted RED curves for pelvic bone from 3D-CRT, IMRT and CK-SBRT	
5.4		39
	(A): Risk-equivalent dose (RED) curves for rectum from 3D-CRT, IMRT and CK-SBRT	
	(B): Differential dose-volume histogram for rectum from 3D-CRT, IMRT and CK-SBRT	
	(C): Volume weighted RED curves for rectum from 3D-CRT, IMRT and CK-SBRT	

LIST OF FIGURES (cont.)

Figure		Page
5.5	(A): Risk-equivalent dose (RED) curves for bladder from 3D-CRT, IMRT and CK-SBRT (B): Differential dose-volume histogram for bladder from 3D-CRT, IMRT and CK-SBRT (C): Volume weighted RED curves for bladder from 3D-CRT, IMRT and CK-SBRT	40
5.6	Relative risk (RR) of SPC for organs in-field and near-field of treatment relative to 3D-CRT or IMRT	44
5.7	Scatter/leakage radiations as a function of distance from tumor center described for 3D-CRT, IMRT and CK-SBRT	46
5.8	Relative risks (RR) of SPC in out-of-field organs relative to 3D-CRT or IMRT	48
5.9	Relative risks (RR) of SPC for imaging dose relative to 3D-CRT or IMRT	52
5.10	Relative risk (RR) of SPC for EAR_{prim}, EAR_{scatt}, and EAR_{image} relative to 3D-CRT or IMRT	56
A.1	Linearity test for TLD-700	77
A.2	Linearity test for TLD-100H.	82

LIST OF ABBREVIATIONS

ABBREVIATIONS	Term
AAA	Analytical anisotropic algorithm
age a	Age attained
age x	Age at exposure
AP	Antero-posterior
ART	Alderson Radiation Therapy
B_s	Backscatter factor
BT	Brachy therapy
CBCT	Cone beam computed tomography
cGy	Centigray
CI	Confidence interval
CK-SBRT	Stereotactic body radiation therapy treated by CyberKnife
cm	Centimeter
cm^2	Square centimeter
cm^3	Cubic centimeter
CT	Computed tomography
D	Prescribed dose
D_{AP}	Imaging dose from x-ray in AP direction for IMRT
D_{CBCT}	Imaging dose from CBCT procedure for IMRT
D_{field}	Imaging dose from treatment field verification for 3D-CRT
D_{image}	Imaging dose
D_{Lat}	Imaging dose from x-ray in lateral direction for IMRT
$D_{scatt/leak}$	Scatter/leakage dose
D_{setup}	Imaging dose from patient setup verification for 3D-CRT

LIST OF ABBREVIATIONS (cont.)

ABBREVIATIONS	Term
$D_{tracking}$	Imaging dose for image-guided procedure for CK-SBRT
dDVH	Differential dose volume histogram
DICOM	Digital imaging and communications in medicine
EAR	Excess absolute risk
EAR_{prim}	Excess absolute risk from primary beam component
EAR_{scatt}	Excess absolute risk from scatter/leakage radiation
EAR_{image}	Excess absolute risk from image-guided procedure
EAR_{total}	Total excess absolute risk
EBRT	External beam radiation therapy
ECC_{ci}	Individual element correction coefficient
ECC_{i}	Element correction coefficient
FOV	Field of view
GTV	Gross tumor volume
Gy	Gray
HR	Hazard ratio
IMRT	Intensity modulated radiation therapy
kg	Kilogram
$k_{Q_{cross}}^{ref}$	Beam quality correction
k_{si}	Individual sensitivity factor
kV	Kilovolt
Lat.	Lateral
LE	Linear exponential model
LNT	Linear no threshold model
LP	Linear plateau model
Lt.	Left
mA	Milliampere

LIST OF ABBREVIATIONS (cont.)

ABBREVIATIONS	Term
mAs	Milliampere second
MeV	Mega-electronvolt
MLCs	Multi leaf collimators
mm	Millimeter
mm^3	Cubic millimeter
MR	Magnetic resonance
ms	Millisecond
mSv	Milli-Sievert
MU	Monitor unit
MV	Megavoltage
NCRP	National Council on Radiation Protection and Measurement
ng/ml	Nanogram per milliliter
$N_{k,Q}$	Calibration coefficient
N_{k,Q_0}^{ref}	Calibration coefficient of ionization chamber
OBI	On-Board Imager
OED	Organ equivalent dose
PET	Positron emission tomography
PTV	Planning target volume
PSA	Prostate-specific antigen
PY	Person-years
$\overline{Q}_{ci}$	Mean of corrected charge integral of standard TLD group
Q_i	Individual charge reading of each TLD
R	Exporsure to Gy conversion factor
RCF	Reader calibration factor

LIST OF ABBREVIATIONS (cont.)

ABBREVIATIONS	Term
RED	Risk-equivalent dose
RP	Radical prostatectomy
RR	Relative risk
RT	Radiation therapy
Rt.	Right
RTOG	Radiation therapy oncology group
SBRT	Stereotactic body radiation therapy
SD	Standard deviation
SEER	Surveillance, Epidemiology, and End Results Program
SPC	Second primary cancer
Sv	Sievert
TLD	Thermoluminescence dosimeter
TPS	Treatment planning system
VMAT	Volumetric modulated arc therapy
V_T	The organ volume
2D-RT	Two-dimensional conventional radiation therapy
3D-CRT	Three-dimensional conformal radiation therapy
˚C	Celsius
μ	Attenuation factor
γ_a	Organ-specific age modifying parameters specified for age attained
γ_e	Organ-specific age modifying parameters specified for age at exposure

CHAPTER I
INTRODUCTION

According to global cancer statistics, prostate cancer is the second most common cancer and the sixth leading cause of death in men [1]. The disease is a major heath concern for the industrialized nations and is an emerging malignancy in the developing countries. The incidence rates vary broadly from > 100 (per 100,000) for the United States, Austria and New Zealand to < 10 for Thailand, Korea and China [2]. Prostate cancer occurs mainly in men aged 65 years or older and is rare before age 40. With the use of prostate-specific antigen (PSA) screening test, the mean age at diagnosis is 67.2 years [3]. Types of prostate cancer management are justified on the basis of PSA level, cancer stage and grade and the comorbidity-adjusted life expectancy [4, 5]. For the localized disease, active surveillance is advised for patients with low risk (i.e. PSA < 10 ng/ml and Gleason score ≤ 6 and T1-T2a stage); prostatectomy or radiotherapy or active surveillance for those with intermediate risk i.e. PSA 10-20 ng/ml or Gleason score 7 or T2b-T2c stage); either radical prostatectomy or external beam therapy (EBRT) is advised for high risk patients (PSA > 20 ng/ml or Gleason score 8-10 or T3-T4 stage) with a realistic prospect of long term disease control, usually patients younger than 75 years [4-6]. From the US registry database (between year 1986-2005), surgery tended to be performed in younger patients (50-59 years) while radiation was chosen for older patients (70-79 years). For patients aged between 60-69 years, the number of patients treated by surgery or radiation were comparable [7]. For localized prostate cancer, surgery and radiation are equivalent in effectiveness [8-10] but have different adverse effect profiles [4, 11]. In high risk patients with microscopic disease extending beyond the prostate, radiation would yield a better control rate than surgery.

Radiotherapy for prostate cancer has evolved from the non-conformal 2-dimensional (2D-RT) radiotherapy to 3-dimensional conformal radiotherapy (3D-CRT) with improved dose conformity. Nowadays, technology for radiation

treatment is highly conformal [such as intensity modulated radiotherapy (IMRT), stereotactic body radiotherapy (SBRT)], capable of generating excellent tumor coverage while greatly reducing doses to organs at risk. Highly precise treatment delivery is made possible by image-guided approach with the aim to assure patient setup, field-size verification or tumor motion tracking. All these features allow tumor dose escalation at an acceptable toxicity profile or facilitating the delivery of hypofractionated treatment in short time [11]. The interest in treating prostate cancer with a hypofractionated scheme based on the observation of a low α/β of 1.5 Gy for this cancer [12, 13] suggesting the tumor is more susceptible to a small number of ablative dose fractions than the use of many conventional fractions of 2 Gy. Lately, effectiveness of the extreme hypofractionation scheme delivered by SBRT was reported for a series of 304 patients with low- (n = 211), intermediated- (n = 81) and high- (n = 12) risk prostate cancer receiving a total dose of 36.25 Gy in 5 fractions of 7.25 Gy. The actuarial 5-year biochemical recurrence-free survival was 97%, 90.7% and 74.1%, respectively and the treatment was well tolerated [14].

Second primary cancer (SPC) development after radiotherapy is a well-conceived subject and is regarded as a serious long-term effect of successful cancer treatment. However, not all SPCs are caused by radiation. According to a population-based study, men with prostate cancer have a greater risk than general population in developing SPC of the bladder, kidney, soft tissue and thyroid particular in these who are diagnosed at young age [15]. SPC with radiation as an etiology has a long latent period and can be detected no sooner then longer than 5 years, arises at sites within or near the treatment field with histology different from primary cancer [16]. Given that the spontaneous SPC tends to develop in sites also described as organs at risks in prostate cancer radiotherapy, how large the effect of radiation treatment affecting SPC incidence rate is a subject of great concern for radiation oncologists. More importantly, how different radiation techniques, e.g. non-conformal RT versus conformal RT, influence SPC induction. A recent systemic review of 19 registry publications, 21 institutional series and 7 independent studies revealed that in relative to surgery, increases in SPC following radiotherapy of prostate cancer were reported by several studies particularly those pertaining to 2D-RT and the risk of SPC tended to increase over time. The significant risk estimated for patients treated with the older

radiation 2D technique (i.e. non-conformal, large field) appeared small, in the range of 1 in 220 to 1 in 290 overall durations of follow-up and might increase to 1 in 70 for patient follow-up to more than 10 years [17]. The most common sites for SPC were observed to locate in the radiation field (in-field sarcoma) and near the field edge (carcinoma of the bladder and rectum) and also at distant site (lung cancer) [18].

The transition from 2D-RT, using large field and non-conformal treatment portal to small field 3D-CRT, or more sophisticated IMRT greatly reduce dose-limiting late tissue complications and probably the SPC risk as well. An institutional study conducted by Huang et al [19] using a match-pair analysis to compare SPC incidence in patients treated with different radiation techniques (2D-RT, brachytherapy (BT), BT boost, 3D-CRT/IMRT; n = 2,955) to those treated by surgery (n = 14,309), they reported, the significant risk for RT after > 5 and > 10 years with hazard ratio (HR) of 1.86 and 4.94, respectively. Of the different RT techniques, only 2D-RT was associated with a significant higher risk (HR = 1.76), not the BT boost (HR = 0.83), 3D-CRT/IMRT (HR = 0.81) or BT monotherapy (HR = 0.53) [19]. The authors acknowledged the small number of patients in each RT subset and the relatively short follow-up time (median 4.96 years for 3D-CRT/IMRT and 9.26 years for 2D-CRT). Despite such insufficiency, the study observed the trend of SPC reduction by BT, BT boost or 3D-CRT/IMRT. The notion that the conformal RT and BT may associate with a lower incidence of SPC in prostate cancer patient is further supported by another institution study with longer follow-up time. Zelefsky et al [20] compared SPC incidence in patients treated with IMRT (n = 897, 7.5 year follow-up), BT (n = 413, 7.7 year follow-up) with radical prostatectomy (RP) (n = 1348, 9.4 year follow-up). Multivariate analysis of predictors for development of SPC revealed that older age ($p = 0.01$) and history of smoking ($p < 0.001$) were significant variables not the type of treatment intervention. The 10-year likelihoods for SPC development in the bladder or rectum estimated for patients treated with IMRT, BT and RP were 4%, 2% and 3%, respectively [20].

Presently, radiotherapy techniques have been developed beyond IMRT toward even more conformal beam technologies for instance stereotactic body radiotherapy (SBRT), volumetric modulated arc therapy (VMAT) and proton beam therapy. The focused beam RT like SBRT is of particular interest in the treatment of

prostate cancer. SBRT is a form of extreme hypofractionation involving a few ablative dose fractions delivered over a few weeks. There is a theoretical advantage of hypofractionation in the treatment of prostate cancer based on its low α/β ratio of 1.5-2 Gy [12, 13] which is lower than 3 Gy of the late rectal complication. Effective biochemical control by SBRT was reported for a series of 304 patients follow out to 6 years [14]. Implication toward the risk of SPC by SBRT in relative to 3D-CRT or IMRT remains unknown and this requires further long-term investigations.

Due to the long latency for solid tumor induction, SPC risk estimation for modern RT relies on theoretical model calculation. Semi-empirical models including the effect of dose fractionation were formulated for the calculation of carcinoma and sarcoma induction [21, 22]. The dosimetric function for cancer induction after RT termed as risk-equivalent dose (RED) was developed based on the linear-quadratic model of cell kill in normal tissues which were unintentionally irradiated. The model describes cancer induction as a function of cell kill per dose fraction (α, β), cumulative dose and repair/repopulation (R) during dose fractionation to account for different carcinogenic susceptibility among organs, organ-specific parameters i.e. α and R were derived from the SPC data of patients treated by RT for Hodgkin's disease. Using the initial slope of dose-response curve and the age-dependent modifying function obtained Japanese A-bomb survivor data, the RED is converted to excess absolute risk (EAR) for a small volume of an organ. EAR for the whole organ (EAR^{org}) is obtained by the summation of EAR for each subvolume based on the differential dose volume histogram of that organ. The dosimetric function RED suggests three possible dose-response relationships, bell-shaped where $R = 0$, plateau $R = 1$ and an in-between relationship $0 < R < 1$. In model fitting, cancer induction curves for most organs are observed to be reasonably fitted by models with neither repair/repopulation of 0% ($R = 0$) nor 100% ($R = 1$) but rather somewhere in between. This observation is in well accord with the findings from a systemic review of the epidemiological studies of the radiation dose-response relationships for organs receiving high dose of fractionated RT (> 5 Gy) where the authors concluded that there were weak supports for a plateau or a downturn type of dose-response function for most solid cancer risk except for SPC of the thyroid gland. Risks of SPC also varied by cancer sites and that combining all sites in risk estimation might conceal differences in carcinogenic susceptibility of

different tissues [23]. EAR^{org} calculation based on the dosimetric function RED would allow the comparison of different radiotherapy treatment plans as a function of differences in dose fractionation (i.e. conventional versus hypofractionation) and dose distribution characterized by dose-volume histogram. The SPC risk ratio for a specific organ in the same patient can also be calculated from the ratio of organ equivalent dose (OED) which was the summation of volume weighted REDs weighted dose variable over the whole organ volume.

Whether the shifting of RT techniques from 3D-CRT to IMRT or a more focused beam SBRT will be reduced to increase the risk of SPC is a subject of continued debate. Hall and Cheng-Shie expressed a concern on the potential increase in SPC risk after the transition from 3D-CRT to IMRT. Since delivery of more conformal radiation doses to the target volume involves using more radiation fields, exposing large volume of normal tissues to lower doses. IMRT also requires longer beam on time leading to greater peripheral whole-body dose from collimator scatter and leakage radiations. At the lower dose level, the risk of SPC is dominated by cell initiation while cell inactivation is less likely to occur. Data of the A-bomb survivors show a linear increase in excess incidence of carcinomas with dose up to about 2.5 Sv [24]. However, those who believe that better dose targeting will lead to SPC reduction since most radiation-induced SPCs arising within or at the margins of the planning target volume [25]. Indeed, reduction in RT volume and field size such as the case of Hodgkin's lymphoma radiotherapy, by replacing the extended field with the involved field technique was observed to be associated with decrease risk of SPC [26].

Modern RT greatly relies on imaging procedures for accurate tumor localization, real-time patient set-up and tumor motion tracking during treatment. Volumetric anatomical imaging procedures have become a routine in image-guided RT as they provide three-dimensional soft tissue information. Daily volumetric imaging has been shown to be effective in reducing systemic and random errors in patient positioning and precise dose delivery. Unlike the treatment dose, the concomitant imaging dose is not target-focused but is widely deposited across the three-dimensional volume of the patient [27]. Modern volumetric imaging procedures, such as these using cone beam CT scans could add 21% - 26% more integral doses to

normal tissues [28]. Consequently, precise delivery of IMRT doses may be achieved at the cost of increase in long-term SPC risk [28].

CHAPTER II
OBJECTIVES

The main objectives:

To assess and compare the impact of 3D-CRT, IMRT and CK-SBRT on risk of second primary cancer (SPC) in organs in or near the treatment field, out-of-field and in image-guided protocols.

The sub-objectives:

1. Risk of SPC in or near the treatment field

1.1 To evaluate how conventional fractionation used in 3D-CRT and IMRT versus hypofractionation used in CK-SBRT affect the dose-risk (RED) relationship.

1.2 To evaluate how different dose-volume relationship affect the shape of the dose-risk curve.

1.3 To calculate the OED and EAR for carcinoma induction in bladder and rectum after treatment by 3D-CRT, IMRT and CK-SBRT.

1.4 To calculate the OED and EAR for sarcoma induction for in-field and near field pelvic soft tissue and pelvic bone after treatment by 3D-CRT, IMRT and CK-SBRT.

2. Risk of SPC from scatter/leakage radiations

2.1 To determine scatter/leakage doses to organs in out-of-field including kidneys, stomach, liver, lung, thyroid and brain from 3D-CRT, IMRT and CK-SBRT.

2.2 To calculate EAR for organs in out-of-field including stomach, liver, lung, thyroid and brain exposed to scatter/leakage radiations from 3D-CRT, IMRT and CK-SBRT.

3. Risk of SPC from image-guided procedures.

3.1 To determine doses from image-guided protocols used in 3D-CRT, IMRT and CK-SBRT.

3.2 To calculate EAR for organs receiving image-guided doses including bladder, rectum, stomach and liver for protocols used in three treatment techniques.

CHAPTER III
LITERATURE REVIEWS

3.1 Second cancer after radiotherapy

Prostate cancer is the second most common cancer in men which radiotherapy is a choice of treatment. Secondary cancer is a concerned long term effect of radiotherapy. The study by Neugut et al [29] analyzed data from the Surveillance, Epidemiology, and End Results Program (SEER) of the US National Cancer Institute from 1973 to 1990. This study was comprised of 141,761 prostate cancer patients (34,889 patients received radiotherapy and 106,872 patients not treated by radiotherapy). After 8 years follow-up, the relative risk of bladder cancer was 1.5 (95% CI 1.1-2.0) for radiotherapy group and 1.0 (95% CI 0.7-1.2) for non-radiotherapy group. At 5 to 8 years, the relative risk of bladder cancer of radiotherapy group was 1.3 (95% CI 1.0-1.7) and non-radiotherapy group was 0.7 (95% CI 0.6-0.9). No significant increase in rectum cancer, acute non-lymphocytic leukemia and chronic lymphocytic leukemia for both groups.

Brenner et al [18] collected data from SEER between 1973 to 1993. They compared secondary cancer risk with 122,123 prostate cancer patients which 51,584 patients were treated by radiotherapy and 70,539 patients were treated by surgery without radiotherapy. This study revealed that 3,549 patients who received radiotherapy developed secondary cancer and 5,055 patients who received surgery developed secondary cancer. The risk of solid tumor increased by 6% in radiotherapy than surgery ($p = 0.02$). For patients who have survival time ≥ 5 years, the increased relative risk reached 15%, and was 34% for patients who have survival time ≥ 10 years. For radiotherapy treatment, the secondary cancer risk increased significant in bladder, rectum, lung and sarcoma within the treatment fields. No significant increase in leukemia. This study estimated absolute risk for secondary cancer after radiotherapy in prostate cancer to be 1 in 290 prostate cancer patients who treated by radiotherapy. For patients survived ≥ 10 years, the risk increased to 1 in 70 patients.

Diallo et al [30] computed about the frequency distribution of secondary cancer sites in relation to irradiated volumes among 115 patients from a cohort of 4,581 patients who developed secondary cancer after childhood cancer radiotherapy. This study classified secondary cancer sites into three categories, as follow: a. a clearly-in-beam region, includes secondary cancer located at more than 2.5 cm inward from the edge of the irradiated volume, b. beam-bordering region, includes secondary cancer located in the volume from 2.5 cm inside to 5 cm outside the irradiated volume, c. distant region, includes secondary cancer outward at more than 5 cm from the irradiated volume. This study reported that clearly-in-beam region which the median dose was 37.1 Gy (7.2 – 63.6 Gy) observed 12% of sarcoma, beam-bordering region which the median dose was 20.1 Gy (0 – 73.1 Gy) observed 66% for sarcoma and carcinoma, and distant region which median dose was 0.3 Gy (0 – 3 Gy) observed 22% of secondary cancer mostly carcinomas. Overall, the most second cancers was 78% observed in the clearly-in-beam and the beam-bordering region. Only 22% of these secondary tumors were observed in distant region.

3.2 Dose-response relationship for second cancer risk

3.2.1 Linear no threshold model (The LNT model)

The linear curve based on the collected data from atomic bomb survivors at Hiroshima and Nagasaki. The atomic bomb survivor data are considered to be the gold standard for estimating cancer risk from radiation because of the large size, the non-selective nature of the radiated population group, the wide range of radiation doses involved, and the long-term systematic monitoring of their health [31]. The LNT model used to estimate the radiation-induced cancer of low dose radiation [32]. The LNT model assumes that cancer risk increases linearly with radiation dose (Figure 3.1). The linear function exists between cancer and dose from about 0.1 Sv up to about 2.5 Sv. National Council on Radiation Protection and Measurements (NCRP) used these data to provide organ specific weighting factors for different organ sites in the body. The total risk for the body is 5%/Sv when the body received equivalent dose.

For radiation dose lower than 2 Gy, the LNT model is used for secondary cancer risk estimation but organ doses in radiotherapy are often received higher than 2 Gy [33].

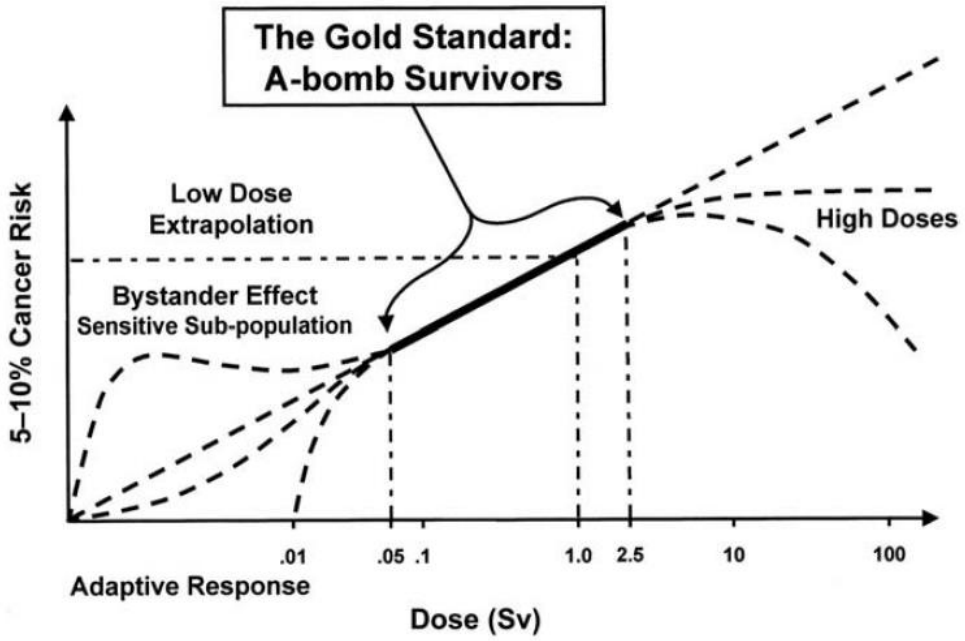

Figure 3.1 The linear dose-response relationship [33].

3.2.2 Linear-exponential model (LE)

The dose response relationship for radiation induced cancer would be bell-shaped which it was introduced by Gray [34]. The bell-shaped were balanced between the induction of transformed cells and cell killing (Figure 3.2). The bell-shaped were explained by the dose response relationship for induction of leukemia in mice which were irradiated for total body. The LE model was used for radiation induced cancer in bone sarcoma [35] and thyroid cancer [36].

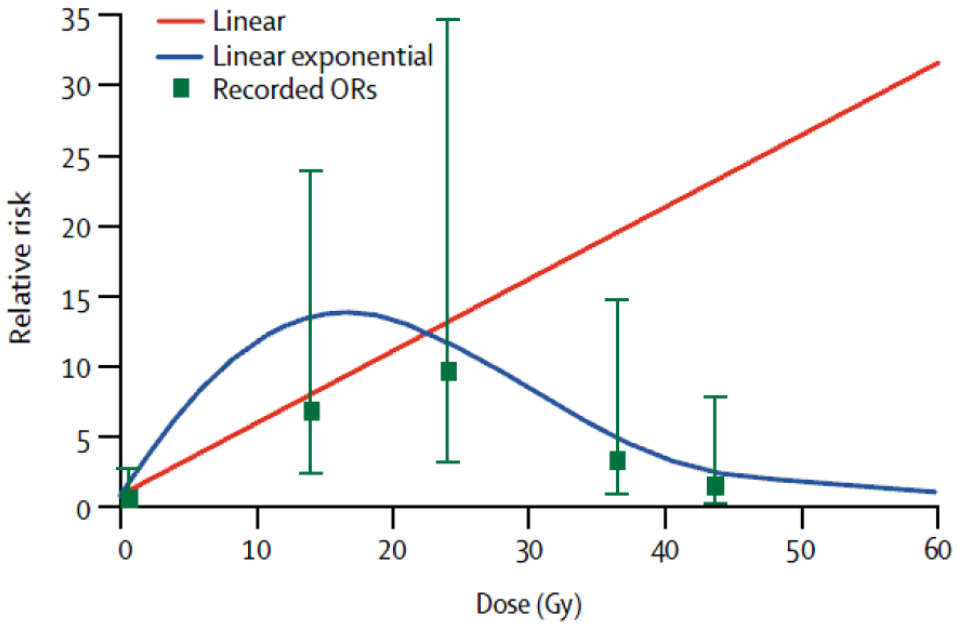

Figure 3.2 The linear-exponential dose-response relationship [36].

3.2.3 Linear-plateau model (LP)

The linear-plateau model is represented by a plateau curve. The curve increases rapidly at low doses and then it does not fall at high doses which it was balanced between the transformed cell and cell killing. The LP model was used for radiation induced cancer in breast, bladder and stomach cancer (Figure 3.3 [33]). Figure 3.2 [36] is shown the comparison of dose-response curve between linear curve, linear-exponential curve and plateau curve [32].

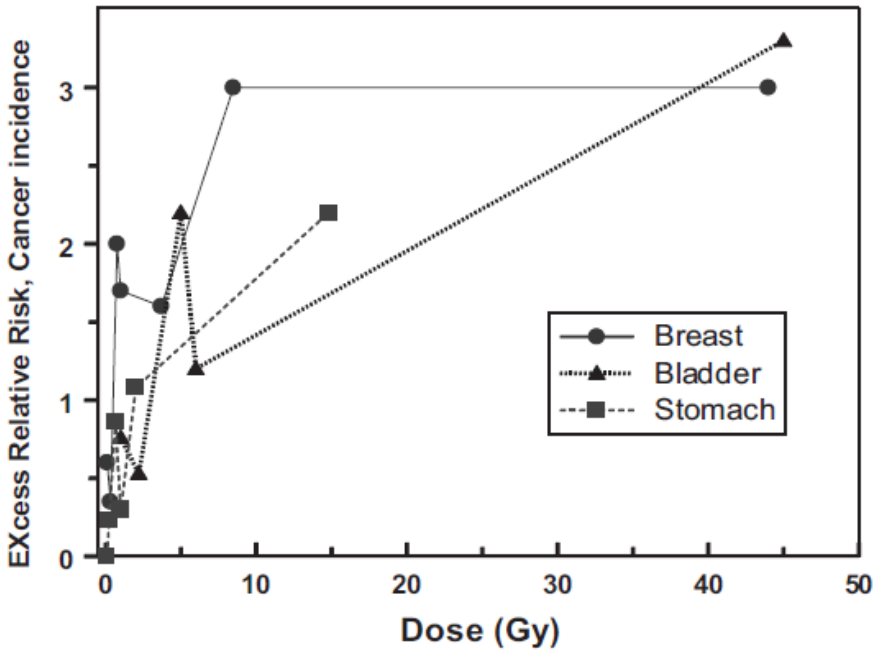

Figure 3.3 The linear-plateau dose-response relationship for breast, bladder and stomach cancer [33].

3.3 Second cancer risk estimation after radiotherapy

Secondary cancer risk from radiotherapy is very small but significantly increased when compared with other treatment [22, 37, 38]. Quantification of secondary cancer risk from radiotherapy is important for prostate cancer patients which have many survived patient from their disease. Schneider et al [39] introduced organ equivalent dose (OED) concept for second cancer risk estimation.

The OED concept used for treatment planning comparisons with regards to cancer induction. The OED based on the epidemiological data of the A-bomb survivors and cancer data on patients receiving radiotherapy for Hodgkin's disease. The concept of OED was defined that the organ will have the same radiation induced cancer incidence when the dose distribution in an organ is equivalent and corresponds to the same OED.

For radiotherapy at high dose, the results of cell killing and cell repopulation are important. For low dose, the OED is the average organ dose, because linear dose-response relationship was used for radiation induced cancer estimation.

The OED was developed to use with organ of interest which have inhomogeneity of dose distributions. The cancer incidence is directly proportional to OED.

The excess absolute risk (EAR^{org}) in an organ was calculated by equation 1 when the dose-volume histogram of that organ is known.

$$EAR^{org} = \frac{1}{V_T}\sum_i V(D_i).\beta.RED(D_i).\mu(\text{age x}, \text{age a}) \quad (1)$$

Where V_T is the total organ volume and V(D) is the sum of all the bins of the dose volume histogram. Risk equivalent dose (RED) is the dose-response relationship for radiation induced cancer in units of dose. β is the initial slope of the dose-response curve at low dose. The modifying function μ is evaluated by equation 2.

$$\mu(\text{age x}, \text{age a}) = \exp\left(\gamma_e(\text{age x} - 30) + \gamma_a \ln\left(\frac{\text{age a}}{70}\right)\right) \quad (2)$$

The fit parameters are gender-averaged and centered at an age at exposure (age x) of 30 years and an attained age (age a) of 70 years. The γ_e and γ_a are the age modifying parameters for a Japanese population and for different sites.

The risk estimation can apply to radiotherapy technique when treatment plan A compare to treatment plan B (respect to cancer induction in one organ and one patient which same gender, age at exposure and age attained) The risk ratio can evaluate by equation 3.

$$\frac{EAR_A^{org}}{EAR_B^{org}} = \frac{\frac{1}{V_T}\sum_i V_A(D_i)\ \beta\ RED(D_i)\ \mu\ (\text{age x}, \text{age a})}{\frac{1}{V_T}\sum_i V_B(D_i)\ \beta\ RED(D_i)\ \mu\ (\text{age x}, \text{age a})} = \frac{OED_A}{OED_B} \quad (3)$$

Where Schneider et al introduced OED which is a dose-response (RED) weighted dose variable averaged over the whole organ volume. OED was calculated by equation 4.

$$OED = \frac{1}{V_T}\sum_i V(D_i)\, RED(D_i) \quad (4)$$

For low dose, RED calculation used linear dose-response model which RED was the average dose for an organ (Equation 5).

$$RED(D) = D \quad (5)$$

For high dose, the RED of carcinoma induction and sarcoma induction which accounts for cell killing and fractionation effects calculated by equation 6 and 7 respectively.

$$RED(D) = \frac{e^{-\alpha' D}}{\alpha' R}\left(1 - 2R + R^2 e^{-\alpha' D} - (1-R)^2 e^{-\frac{\alpha' R}{1-R}D}\right) \quad (6)$$

$$RED(D) = \frac{e^{-\alpha' D}}{\alpha' R}\left(1 - 2R + R^2 e^{\alpha' D} - (1-R)^2 e^{-\frac{\alpha' R}{1-R}D} - \alpha' RD\right) \quad (7)$$

Where the tissue is irradiated with fractionated treatment schedule of dose fractions d up to a dose D. R is the repair/repopulation parameter. The α' is defined by using the linear quadratic model which is evaluated by equation 8.

$$\alpha' = \alpha + \beta D = \alpha + \beta \frac{D}{D_T} d_T \quad (8)$$

Schneider et al compared the risk of secondary cancer after radiotherapy in prostate cancer between 3D-CRT and IMRT by using OED concept. The treatment plans were calculated for 3D-CRT and IMRT in 15 MV and 18 MV photons. Thirty prostate cancer patients were estimated based on OED with a linear-exponential and a plateau dose-response curve. Differential dose volume histograms (dDVHs) were calculated from 3D dose distribution in CT volume. Scatter dose was estimated from measurement at point 50 cm from the center of 10x10 cm^2 treatment field at 10 cm depth. Both of the primary beam components and the scatter dose components were used to estimate OED by using a linear-exponential model and a plateau model.

For 3D-CRT and IMRT comparison in a linear-exponential model revealed that OED of primary dose for IMRT increased secondary cancer risk more than 3D-CRT was 1.18 times and 1.21 times in 15 MV and 18 MV respectively. For primary dose in a plateau model, In 15 MV 3D-CRT increased secondary cancer risk more than IMRT was 1.05 times, but in 18 MV, IMRT increased secondary cancer risk more than 3D-CRT for 1.02 times.

For scatter dose component, secondary cancer risk comparison between 3D-CRT and IMRT by using a linear-exponential model revealed that IMRT increased risk more than 3D-CRT 1.5 times and 1.44 times in 15 MV and 18 MV respectively. For a plateau model, IMRT increased secondary cancer risk more than 3D-CRT was 1.5 times and 1.47 times in 15 MV and 18 MV, respectively.

For linear-exponential model, the OED total (including OED value from primary beam component and scatter dose component) of IMRT was 1.2 times for 15 MV and 1.29 times for 18 MV compared with 3D-CRT. In a plateau model, the OED total of IMRT was 1.02 times for 15 MV and 1.14 times for 18 MV more than 3D-CRT.

3.4 Imaging radiation dose for radiotherapy

Monica et al [40] studied about imaging dose from CBCT by TLD measurement. TLD were inserted into 26 organs (the organ selected by using ICRP 60) in female anthropomorphic phantom. The protocol of CBCT at pelvis region is half-fan, 40 cm field of view (FOV), 2.5 mm thickness and 13.7 cm longitudinal extent. CBCT scan used 125 kV, 80 mA and 25 ms. The primary x-ray beam covered the ovary, uterus, small intestine, bone marrow in iliac crest, colon, bladder and skin. The absorbed dose of in-field organ varied from 3.8 cGy to 6.2 cGy per one scan and skin dose was 5.4 cGy. The mean absorbed dose per scan of gonads, colon, bladder, and rectum were 0.84, 1.18, 1.20, and 0.88 cGy, respectively. The effective dose to the body was 22.7 mSv. CBCT scan adds radiation dose to the patient which increase the risks of secondary cancers. From ICRP 60, the probability of inducing fatal cancer from a single radiographic exposure is $5x10^{-5}$ per mSv which based on the linear no threshold model. When prostate cancer patient received radiation dose from CBCT

standard mode for 35 fractions, the patient received an effective dose of 800 mSv which can increase secondary cancer risk for 4%.

CHAPTER IV
MATERIALS AND METHODS

4.1 Prostate treatment plans

Three treatment plans, 3D-CRT plan, IMRT plan and CK-SBRT plan, were generated for 6 patients with localized tumor of the prostate gland. The average gross tumor volume (GTV) was 47.80 cm^3 (range 36.64 – 62.01 cm^3). In planning, CT images of the same patient were imported to treatment planning computer. Tumor and organs at risk including bladder, rectum, bowel, and pelvic bone were contoured by experienced radiation oncologist. The planning data of 3D-CRT, IMRT and CK-SBRT are showed in Table 4.1, 4.2 and 4.3 and the CK-SBRT treatment delivered by linac on robotic arm by Accuray CyberKnife G4 System (Accuray Incorporated, Sunnyvale, California, USA). The 3D-CRT and IMRT treatments were delivered by Clinac iX linear accelerator (Varian Oncology Systems, Palo Alto, California). Details for the three treatment plans are presented in Tables 4.1-4.3.

Table 4.1 The 3D-CRT planning data for six prostate cancer patients

Variable	Patient Number					
	1	2	3	4	5	6
GTV (cm^3)	62.01	44.42	44.88	43.71	55.11	36.64
PTV (cm^3)	133.16	107.66	108.08	109.19	120.93	92.89
Beam energy (MV)	10	10	10	10	10	10
Prescribed dose (Gy)	78	78	78	78	78	78
Dose/Fraction (Gy)	2	2	2	2	2	2
No. Fraction	39	39	39	39	39	39
Field size (cm^2)	8.3x7.6	7.8x8.0	8.4x7.1	8.5x6.9	8.4x7.2	8.1x5.8
No. Beam orientation	7	7	7	7	7	7
Max Dose	80.40	81.00	82.00	81.80	81.00	81.40
Total treatment MU	11154	11739	11154	11505	11934	12675
No. Image-guided	23	23	23	23	23	23

Table 4.2 The IMRT planning data for six prostate cancer patients

Variable	Patient Number					
	1	2	3	4	5	6
GTV (cm^3)	61.90	44.42	44.82	43.71	55.11	36.64
PTV (cm^3)	149.51	118.02	123.63	123.52	140.92	105.20
Beam energy (MV)	6	6	6	6	6	6
Prescribed dose (Gy)	78	78	78	78	78	78
Dose/Fraction (Gy)	2	2	2	2	2	2
No. Fraction	39	39	39	39	39	39
Field size (cm^2)	9.5x8.3	9.3x8.3	10.8x8.0	9.8x7.1	10.0x7.8	9.6x6.1
No. Beam orientation	9	9	9	9	9	9
Max Dose	81.80	81.80	81.80	81.80	81.80	81.80
Total treatment MU	29133	27261	26598	31005	27066	29211
No. Image-guided	86	86	86	86	86	86

Table 4.3 The CK-SBRT planning data for six prostate cancer patients

Variable	Patient Number					
	1	2	3	4	5	6
GTV (cm^3)	62.01	44.42	44.88	43.71	55.11	36.64
PTV (cm^3)	95.84	84.25	84.81	78.61	97.96	69.23
Beam energy (MV)	6	6	6	6	6	6
Prescribed dose (Gy)	36.25	36.25	36.25	36.25	36.25	36.25
Dose/Fraction (Gy)	7.25	7.25	7.25	7.25	7.25	7.25
No. Fraction	5	5	5	5	5	5
Collimator size (mm)	15,35	15,30	20,30	20,35	15,30	12.5,35
No. Beam orientation	289	285	184	252	245	246
Max Dose	45.31	45.31	45.89	44.75	44.75	45.31
Total treatment MU	40175	50488	40616	35295	50420	48575
No. Image-guided	1275	1220	1015	1195	1145	880

4.2 Computerized Treatment Planning System (TPS)

3D-CRT and IMRT treatment plans were generated by Eclipse TPS version 8.9.21 (Varian Medical System, Palo Alto, California, USA). The system consists of the DELL Precision 490 workstation and is run by the XP professional. The 3D-CRT and IMRT planning used AAA algorithm for dose distribution and the plans were transferred to Clinac iX linear accelerator treatment machine.

The MultiPlan TPS (Accuray Incorporated, Sunnyvale, California, USA) was used to generate SBRT treatment plan. The system used the volumetric CT image for the determination of beam position. The MultiPlan TPS runs on Window XP operating system (Microsoft Corporation, Redmond, Washington, USA). The system uses ray tracing, Clarkson and superposition algorithm to calculate dose distribution to allow displaying of DVH for region or organ of interest.

4.3 Treatment Machine

4.3.1 Linear Accelerator (Linac)

Clinac iX linear accelerator (Varian Oncology Systems, Palo Alto, California) was used for 3D-CRT and IMRT treatment. The Clinac iX can generate two photon energies 6 MV, 10 MV and five electron energies 6 MeV, 9 MeV, 12MeV, 15 MeV and 22 MeV. The machine dose rates are 100, 200, 300, 400, 500 and 600 MU per minute. At a distance from the source to isocenter of 100 cm, the field size for the photon beam can be continuously changed from 0.5 x 0.5 cm^2 to 40 x 40 cm^2. The Clinac iX machine has two main components including gantry and On-Board Imager (OBI). The gantry consists of Linear accelerator system for producing photon and electron beams. The collimating system is a total of 120 leaf collimators arranged as two sets of 60 leaf collimators, positioning in perpendicular to the beam path. In each collimator set, the collimator leaves are aligned side by side. Thickness of the collimator leaflet is 1 cm except for 40 leaflets these in the central zone which have a thickness of 0.5 cm. The OBI consists of a flat panel detector and a kV x-ray tube mounted on the gantry of Clinac iX. The OBI can take kV image and CBCT image that matching the reference images for patient position verification before treatment [41]. Clinac iX linear accelerator is shown in Figure 4.1.

Figure 4.1 Clinac iX linear accelerator

4.3.2 Accuray CyberKnife G4 System

The Accuray CyberKnife G4 System ® Robotic Radiosurgery System (Accuray Incorporated, Sunnyvale, CA, USA) consists of two parts including a lightweight 6 MV linear accelerator mounted on a robotic manipulator and the target-locating system. It can produce a 6 MV x-ray treatment beam with dose rate up to 600 MU per minute. Beam collimation is done via a fixed circular collimator. There are 12 collimators with the sizes ranging between 5-60 mm at 80 cm from source to axis distance. This machine can be moved by using six axis joints on robotic arm for tumor irradiation. Precise target location is achieved by a target-location system consisting two kilo-voltage x-ray sources mounting on the ceiling and two amorphous silicon flat panel digital detectors positioning on the floor. A high resolution digital square image (1,024 x 1,024 pixels) is generated by the two x-ray sources projecting at 45˚ from the vertical axis onto the detector plane. The x-ray image guidance of CyberKnife can verify patient position by four tracking methods including fiducial tracking method, skull tracking method, synchrony tracking method and X-sight spine tracking method [42]. CyberKnife machine is shown in Figure 4.2.

Figure 4.2 Accuray CyberKnife G4 System

4.4 Thermoluminescence dosimeter (TLD)

4.4.1 Thermoluminescence dosimeter type 700 rods (TLD-700)

TLD-700 rods (Harshaw Chemical Company, Cleveland, Ohio) were used for the measurement of scattered and leakage doses (Figure 4.3). The density of TLD-700 rod is nearly tissue equivalent and consists of Lithium fluoride (7Li: 6Li was 99.99%: 0.01%) doped with magnesium and titanium (LiF:Mg,Ti). The size of TLD-700 rod is 1 mm in diameter and 6 mm in length and can measure dose in range 10 pGy to 10 Gy [43].

Figure 4.3 Thermoluminescence dosimeter types 700 rods in planchet

4.4.2 Thermoluminescence dosimeter type 100H chips (TLD-100H)

TLD-100H chips (Harshaw Chemical Company, Cleveland, Ohio, Figure 4.4) were used for measurement of doses from diagnostic imaging for its high sensitivity to low doses and weak energy dependent between 40 to 125 kV_p [44]. TLD-100H chips with a dimension of 3.2 x 3.2 x 3.2 mm^3 has an effective atomic number of 8.2, nearly tissue equivalent [45]. The measurable dose range for TLD-100H chips was between 10 pGy to 10 Gy.

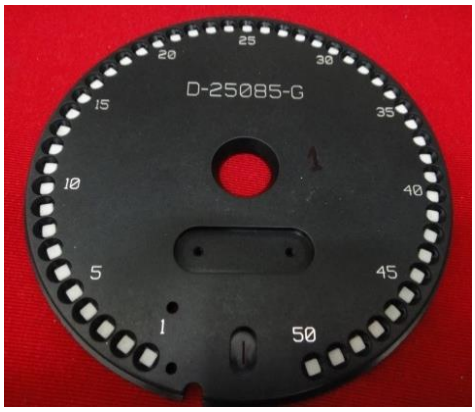

Figure 4.4 Thermoluminescence dosimeter types 100H chips in planchet

4.4.3 Thermoluminescence dosimeter reader system

Dose measured with TLD-700 rods and TLD-100H chips were read out by the TLD read system consisting of the TLD reader (HARSHAW TLD Model 5500 Automatic Reader, Figure 4.5) and TLD annealing oven (PTW-TLDO, Figure 4.6). TLD reader system can take TLD up to 50 chips or rods on a planchet in one time and can measure dose in the range of 10 uGy to 20 Gy [43]. TLDs reader is controlled by WinREMS program which it set different parameter between TLD-700 rods and TLD-100H chips (Table 4.4).

Table 4.4 Preheat and annealing parameters for TLD-700 rods and TLD-100H chips

Parameter	TLD-700	TLD-100H
Preheat		
• Temperature	100 ˚C	145 ˚C
• Heating time	10 minutes	10 seconds
• Reading time	23 1/3 seconds	26 2/3 seconds
Annealing		
• Maximum temperature	400 ˚C	400 ˚C
• Heating time	4 hour	4 hour

Figure 4.5 Thermoluminescence dosimeter reader

Before and after irradiation, the TLDs were heated in the annealing oven at temperatures and time precisely set and controlled by THELDO software which is a microprocessor-controlled software (Table 4.4).

Figure 4.6 Thermoluminescence annealing oven

4.5 The Female Alderson Radiation Therapy Phantom (ART)

The phantom used for dose measurement is the female Alderson radiation therapy phantom (Figure 4.7) made of materials which are tissue-equivalent. The size of this phantom is 155 cm tall, 50 kg weight. The female ART phantom is intersected in 33 axial slabs of 2.5 cm thick except the first and the last slab is thicker than 2.5 cm

and not used for dose measurement. In each slab, there are holes for insertion of tissue equivalent pins (such as bone equivalent, soft tissue equivalent, lung equivalent) and TLD holder pins [46].

Figure 4.7 The Female Alderson Radiation Therapy Phantom

4.6 Treatment planning

CT scan or MR images from each patient were recorded in DICOM files and imported to Eclipse TPS for 3D-CRT and IMRT planning and to MultiPlan TPS for CK-SBRT planning. Contours of GTV, PTV, bladder and rectum were drawn by radiation oncologist. To define the PTV margins for 3D-CRT and IMRT, 7 mm and 8 mm were added to GTV in all directions except for the posterior margins where 5 mm were added according to Radiation Therapy Oncology Group 0415 (RTOG 0415) [47]. This was in contrast to CK-SBRT plan where 1-2 mm were added to the GTV. The treatment plan acceptance criteria were as follow: For 3D-CRT and IMRT, the PTV should receive no less 95% of the prescribed dose and doses to organs at risk not exceeding the tolerance doses stated in RTOG 0415. For CK-SBRT, an 80%

isodose coverage was assigned for PTV with hot spots of less than 110% of prescribed dose. Doses to organs at risk were within the dose constraints suggested by Timmerman [48].

The optimized planning details regarding beam energy, beam number and orientation, prescription dose, fraction size and treatment MUs are presented in Table 4.1 to Table 4.3.

Differential dose volume histogram (dDVHs) were calculated for PTV representing in-field pelvic soft tissue, bladder, rectum, bowels, pelvic bone, and the remainder pelvic soft tissue or the near-field pelvic soft tissue (total scan volume minus prostate, bladder, rectum, pelvic bone and bowels).

4.7 Second cancer risk calculation for organs in or near the treatment field

A dose-response model incorporates cell killing, fractionation and repair/repopulation effects developed by Schneider et al [22] was adopted for this study. This mechanistic dosimetric function termed as risk equivalent dose (RED) is formulated for carcinoma risk and sarcoma risk as well. RED for carcinoma induction can be calculated as follow:

$$\mathrm{RED}_{\mathrm{carcinoma}} = \frac{e^{-\alpha' D}}{\alpha' R}\left[1 - 2R + R^2 e^{\alpha' D} - (1-R)^2 e^{\frac{-\alpha' R D}{1-R}}\right] \qquad (1)$$

Where it assumed that the tissue is irradiated with a fractionated treatment scheme of equal dose fractions d up to a dose D. R is the tissue specific repair/repopulation factor and α' is the cell kill parameter per dose fraction d is obtained from the tissue-dependent parameters of the linear quadratic model.

$$\alpha' = \alpha\left[1 + \frac{d_T}{\alpha/\beta}.\frac{D}{D_T}\right] \qquad (2)$$

Where D_T and d_T are prescribed dose and dose fraction to target volume. In fact, D_T/d_T yields the number of dose fractions n for a particular dose fractionation

schedule. α/β for SPC induction is 3 Gy for all tissue types [22]. As the cancer induction curves are insensitive to changes in α/β over a broad range of 1 - 15 Gy [49-51].

Therefore $$\alpha' = \alpha\left[1 + \frac{D}{3n}\right]$$

Where D/n is d Gy per fraction.

Similarly, RED for sarcoma induction can be calculated as follows:

$$RED_{sarcoma} = \frac{e^{-\alpha' D}}{\alpha' R}\left[1 - 2R + R^2 e^{\alpha' D} - (1-R)^2 e^{\frac{-\alpha' RD}{1-R}} - \alpha' RD\right] \quad (3)$$

Based on these mechanistic formulations, RED would allow the risk assessment for treatment with different fractionation schemes, i.e. the conventional fractionation used in 3D-CRT and IMRT versus the hypofractionation used in CK-SBRT.

Tissues closed to the treatment field typically receive inhomogeneous dose distribution. The concept of organ equivalent dose (OED) was employed to calculate the SPC induction in an organ receiving heterogeneous doses [39]. On the basis of differential dose-volume histogram, RED was calculated for each voxel V(Di). The sum over all voxel weighted RED divided by the organ volume (V_T) yields the OED as follow:

$$OED = \frac{1}{V_T}\sum V(D_i).RED(D_i) \quad (4)$$

For 3D-CRT and IMRT, $V(D_i)RED(D_i)$ was calculated at dose bin of 0.2 Gy. While 0.45 Gy/per dose bin was decided for CK-SBRT.

Excess absolute risk (EAR) for prostate cancer patient is factorized into a function of dose $RED(D_i)$ in a small volume element $V(D_i)$ and a modifying function (μ) dependent on age at exposure (age x) and age attained (age a).

$$EAR\ (D_i, \text{age x}, \text{age a}) = \beta\ .\ RED(D_i)\ .\ \mu(\text{age x}, \text{age a}) \quad (5)$$

Where β is the initial slope of the dose-risk curve and expressed as an organ specific excess cases per 10,000 person-years (PY) gray (Gy). The function μ contains the population dependent variables:

$$\mu(\text{age x, age a}) = \exp\left[\gamma_e\,(\text{age x} - 30) + \gamma_a \ln(\text{age a}/70)\right] \quad (6)$$

Where γ_e and γ_a are organ-specific age modifying parameters specified for age at exposure and age attained, respectively.

EAR for the whole organ (EAR^{org}) can be calculated data obtained from using the differential dose volume histogram.

$$EAR^{org} = \frac{1}{V_T}\sum V(D_i)\cdot\beta\cdot RED(D_i)\cdot\mu(\text{age x, age a}) \quad (7)$$

Parameters for RED and EAR calculation are presented in Table 4.5. To allow an insight into the impact of the shift from 3D-CRT to IMRT and CK-SBRT, all EAR values were calculated for a representative patient irradiated at age 60 years and attaining an age at 80 years.

Table 4.5 Parameters for RED and EAR calculations [17, 22]

Organ	RED calculation			EAR calculation		
	α (Gy^{-1})	α/β (Gy)	R	$\beta(10^4 PYGy)^{-1}$	γ_e (y)	γ_a (y)
Pelvic soft tissue	0.060	3	0.50	0.60	-0.013	-0.56
Pelvic bone	0.067	3	0.50	0.20	-0.013	-0.56
Bladder	0.219	3	0.06	3.80	-0.024	2.38
Rectum	0.033	3	0.56	0.73	-0.056	6.90

4.8 Second cancer risk from out-of-field radiations

4.8.1 Measurement of scatter/leakage radiation

$\overline{D}_{scatt/leak}$ was scatter/leakage dose from primary radiation which was measured by placing TLD-700 rods at 9 locations in ART phantom as described in Table 4.6 and Figure 4.8. The 9 locations included brain, thyroid, lung, liver, stomach and kidney in ART phantom (Table 4.6).

With similar patient treatment position and treatment plan, scatter/leakage doses were measured for 3D-CRT plan with a phantom dose of 10 Gy from 10 MV photon, IMRT plan 10 Gy of 6 MV and CK-SBRT 5 Gy of 6 MV. The measurements were repeated 3 times. The average scatter/leakage dose measured in Gy for each treatment plan was divided by the MU used for phantom irradiation. The Gy/MU thus obtained was used for the calculation of $\overline{D}_{scatt/leak}$ for organs listed above by multiplying the Gy/MU with the total MU used for treating each patient.

Table 4.6 Nine locations of TLD in ART phantom for scatter/leakage dose measurement

Number	Organ	Slab number	Distance from tumor center (cm)
1	Brain	2	70.0
2	Rt. thyroid	8	54.0
3	Lt. thyroid	8	54.0
4	Rt. lung	14	38.8
5	Lt. lung	14	38.8
6	Liver	18	28.5
7	Stomach	18	25.5
8	Rt. kidney	21	20.7
9	Lt. kidney	21	20.7

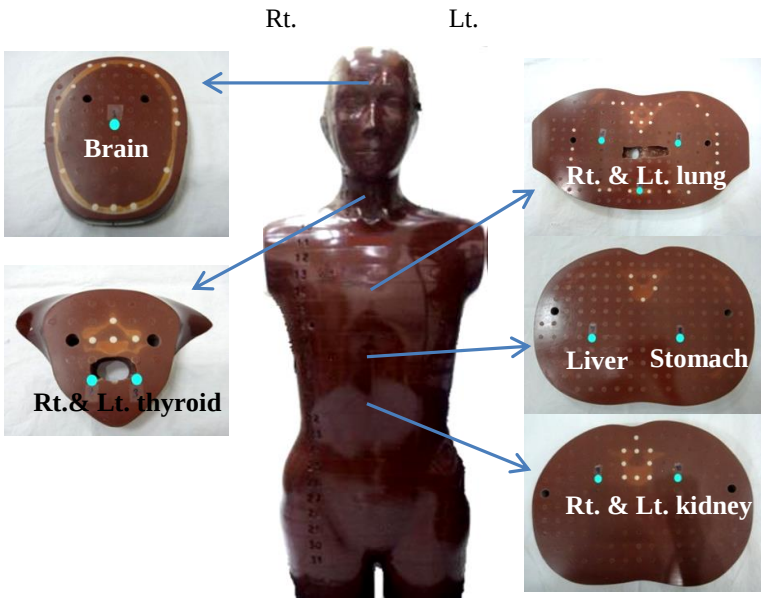

Figure 4.8 Position of TLDs in ART phantom for scatter/leakage dose measurement

4.8.2 EAR calculation for organs receiving scatter/leakage doses

A linear model was applied for the low dose out-of-field regions [22].

$$RED(D) = D_i \quad (8)$$

And

$$EAR^{org} = \beta \cdot RED \cdot \mu(\text{age x, age a}) \quad (9)$$

Parameters for EAR calculation are available for brain, thyroid, lung, liver and stomach (Table 4.7).

Table 4.7 Parameters for EAR calculations for organs in out-of-field regions [22]

Organ	β (10^4PYGy)$^{-1}$	γ_e (y)	γ_a (y)
Brain	0.7	-0.024	2.38
Thyroid	0.4	-0.046	0.60
Lung	8.0	0.002	4.23
Liver	2.4	-0.021	3.60
Stomach	5.2	-0.002	7.90

4.9 Second cancer risk from image-guided procedures

4.9.1 Measurement of radiation doses from image-guided procedures

Details of image-guided protocols for 3D-CRT, IMRT and CK-SBRT are shown in Table 4.8. Each measurement was repeated 3 times.

Table 4.8 Image-guided protocols and phantom measurement

Treatment Technique	Image-guided protocol	Field size	Image number / measurement
3D-CRT	Shape of treatment field		
	• 7 images, 10 MV, 7MU	Range5.8-8.5cm	5 images
	Setup verification (AP, lateral)		
	• 16 images, 10 MV, 16 MU	20 x 26 cm^2	5 images
IMRT	Setup verification		
	Cone beam CT (CBCT)		
	• 10 circular turns, 125 kV, 1mAs	16 cm circular beam	5 circular turns
	AP		
	• 38 images, 75 kV, 16 mAs	20 x 26 cm^2	40 images
	Rt. lateral		
	• 38 images, 105 kV, 80 mAs	20 x 26 cm^2	40 images
CK-SBRT	Tumor tracking x-ray projection		
	• 1122 (880-1275) images, 120 kV, 10mAs	59 x 66 cm^2	150 images

Doses from imaging procedures were measured using TLD-700 rods for 3D-CRT, TLD-100H chips for IMRT and CK-SBRT placed in phantom at locations corresponding to prostate, bladder, rectum, stomach, liver and kidney (Table 4.9, Figure 4.9).

Table 4.9 Points of imaging dose measurement in ART phantom

Treatment Technique	Imaging dose		Scatter dose
	$\overline{D}_{image}$	Point of measurement	Point of measurement
3D-CRT	$\overline{D}_{field}$, $\overline{D}_{setup}$	Prostate, bladder, rectum, liver, stomach, kidney	Brain, thyroids, lungs
IMRT	$\overline{D}_{CBCT}$, $\overline{D}_{AP}$, $\overline{D}_{Lat}$	Prostate, bladder, rectum, liver, stomach, kidney	Brain, thyroids, lungs
CK-SBRT	$\overline{D}_{tracking}$	Prostate, bladder, rectum, liver, stomach, kidney	Brain, thyroids, lungs

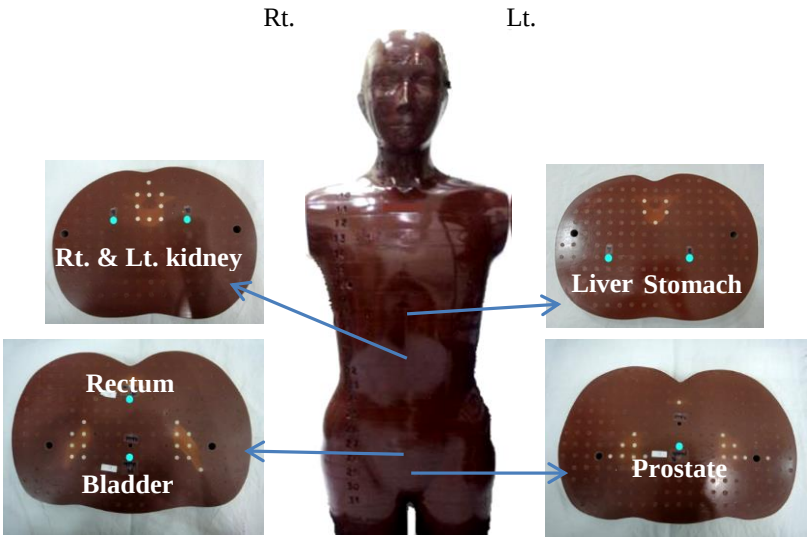

Figure 4.9 TLD positions for imaging dose measurement of 3D-CRT, IMRT and CK-SBRT

4.9.2 EAR calculation for organs receiving imaging doses

Based on the linear model for low dose regions, RED(D) was proportional to the imaging dose D which was the sum of doses from the entire protocol. The EARs for exposed organs were calculated using parameters shown in Table 4.5 and Table 4.7.

4.10 Comparison of second cancer risks between treatments and statistical analysis.

For a patient (same age at exposure and age attained), the relative risk (RR) which was the SPC risk for treatment modality A in relative to modality B can be assessed as follow [22]:

$$\mathrm{RR} = \frac{\mathrm{EAR}_{\mathrm{A}}^{\mathrm{org}}}{\mathrm{EAR}_{\mathrm{B}}^{\mathrm{org}}} = \frac{\mathrm{OED}_{\mathrm{A}}}{\mathrm{OED}_{\mathrm{B}}} \tag{10}$$

The difference between treatment modality OEDs was analyzed by student paired t-test. All the statistical tests were two-tailed and $p \leq 0.05$ was considered statistically significant.

CHAPTER V
RESULTS

5.1 SPC risks for organs in or near the treatment field

5.1.1 Dose-risk relationship and effect of dose-fractionation

Risk equivalent dose (RED), dose volume histogram and dose-volume weighted by RED for organ in or near treatment field from 3D-CRT, IMRT and CK-SBRT are showed in Tables 5.1 (A–C) – 5.7 (A–C).

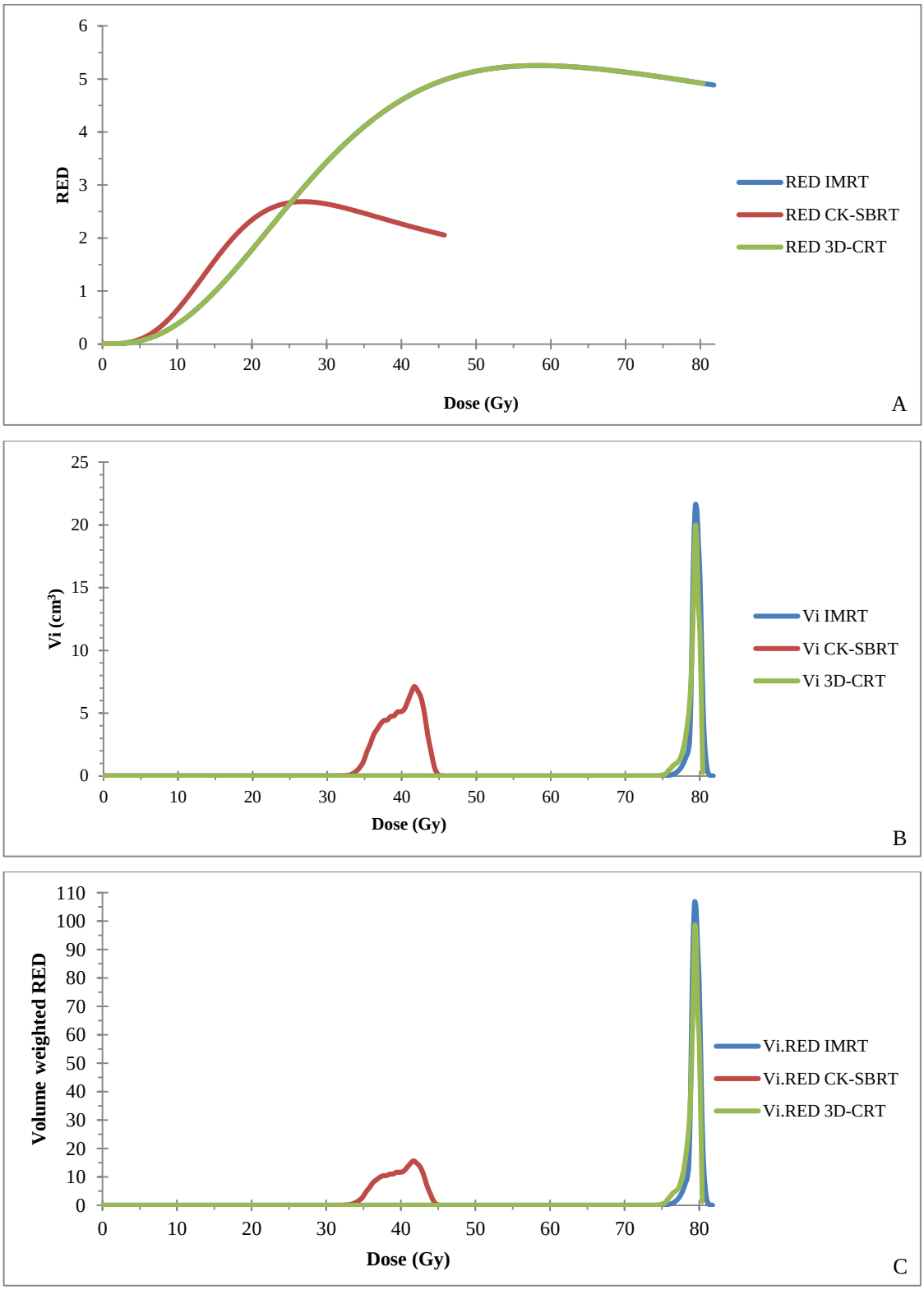

Figure 5.1 (A) Risk-equivalent dose (RED) curves, (B) Differential dose-volume histogram, (C) Volume weighted RED curves for in-field pelvic soft tissue from 3D-CRT, IMRT and CK-SBRT plans

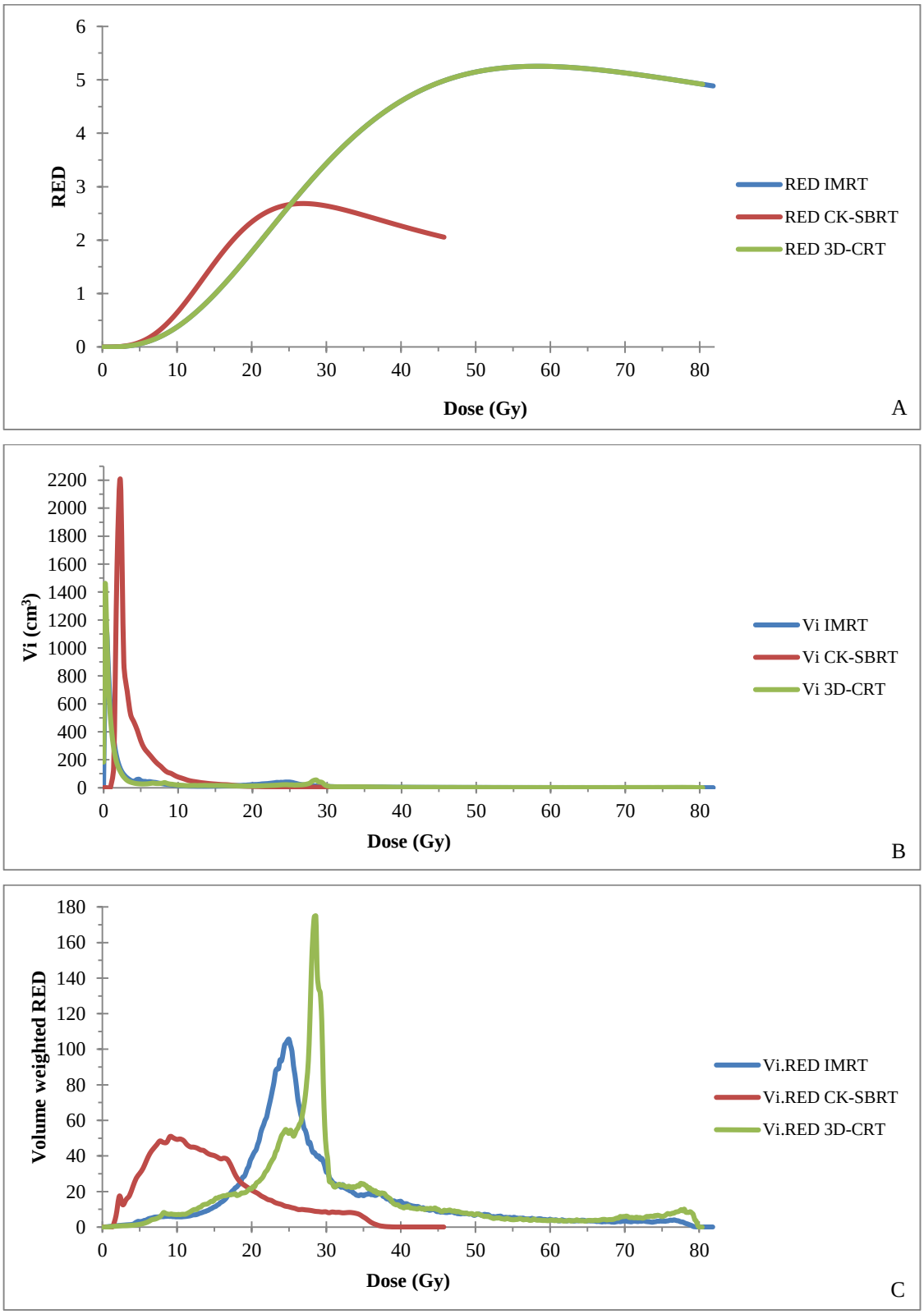

Figure 5.2 (A) Risk-equivalent dose (RED) curves, (B) Differential dose-volume histogram, (C) Volume weighted RED curves for near-field pelvic soft tissue from 3D-CRT, IMRT and CK-SBRT plans

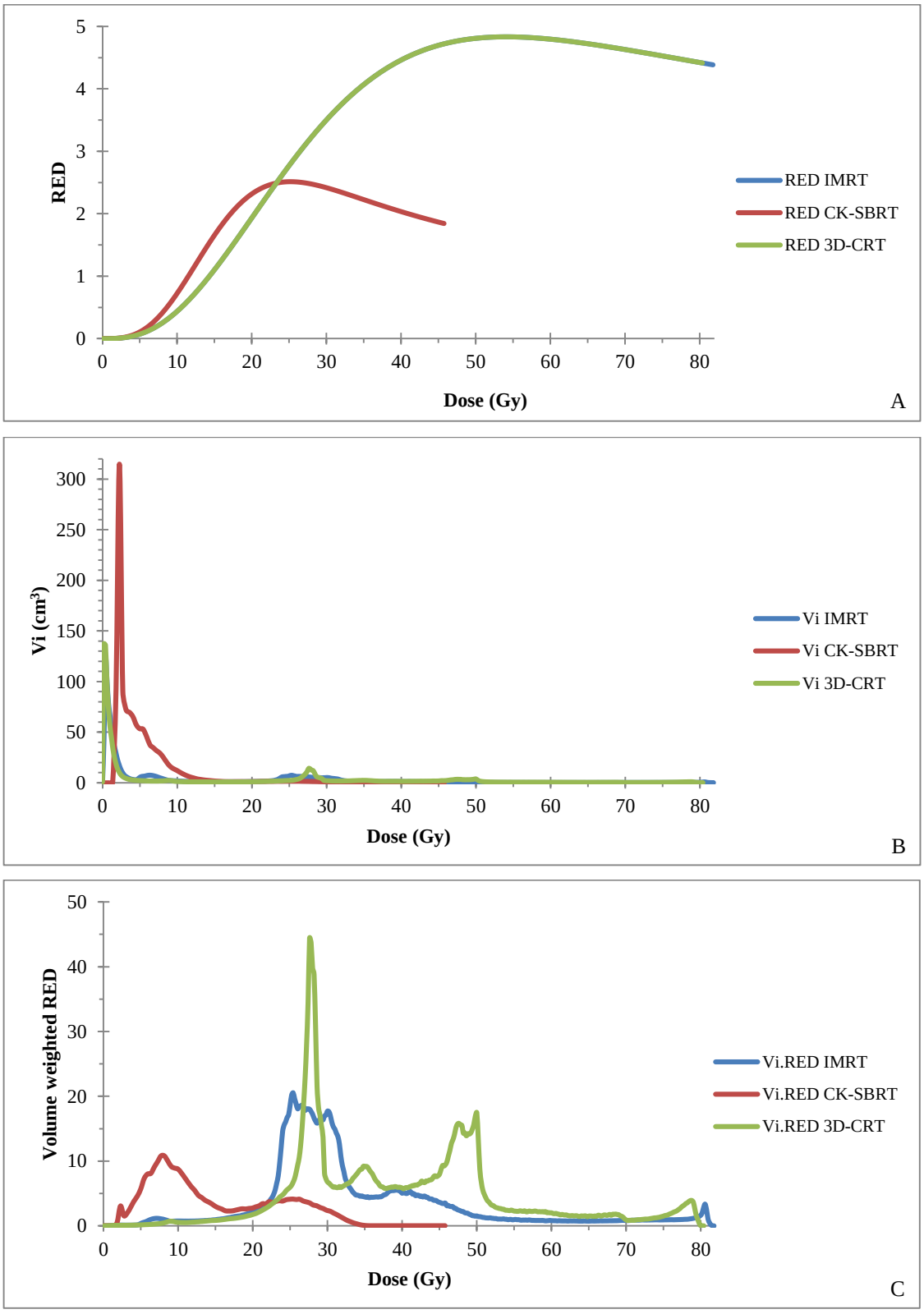

Figure 5.3 (A) Risk-equivalent dose (RED) curves, (B) Differential dose-volume histogram, (C) Volume weighted RED curves for pelvic bone from 3D-CRT, IMRT and CK-SBRT plans

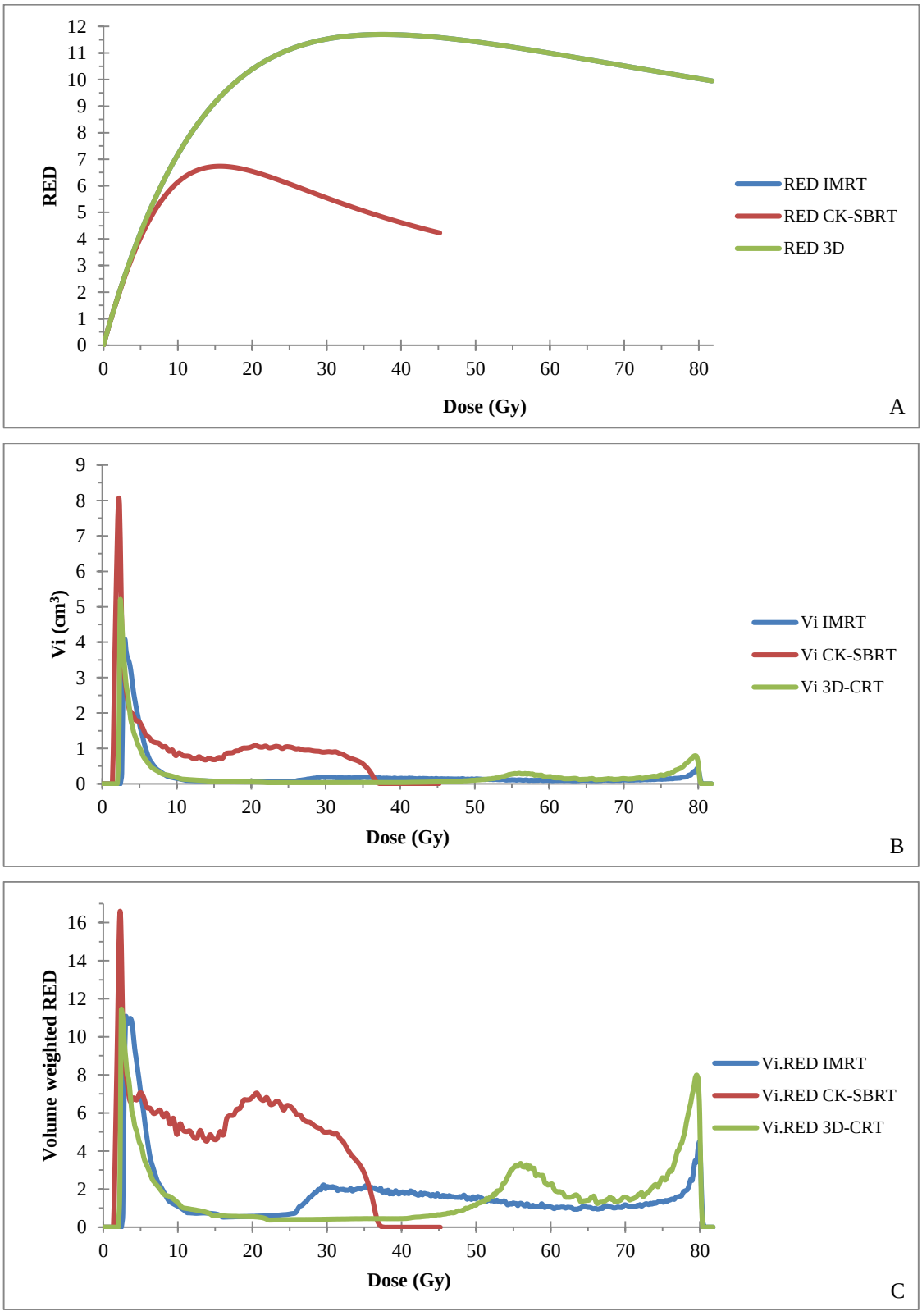

Figure 5.4 (A) Risk-equivalent dose (RED) curves, (B) Differential dose-volume histogram, (C) Volume weighted RED curves for rectum from 3D-CRT, IMRT and CK-SBRT plans

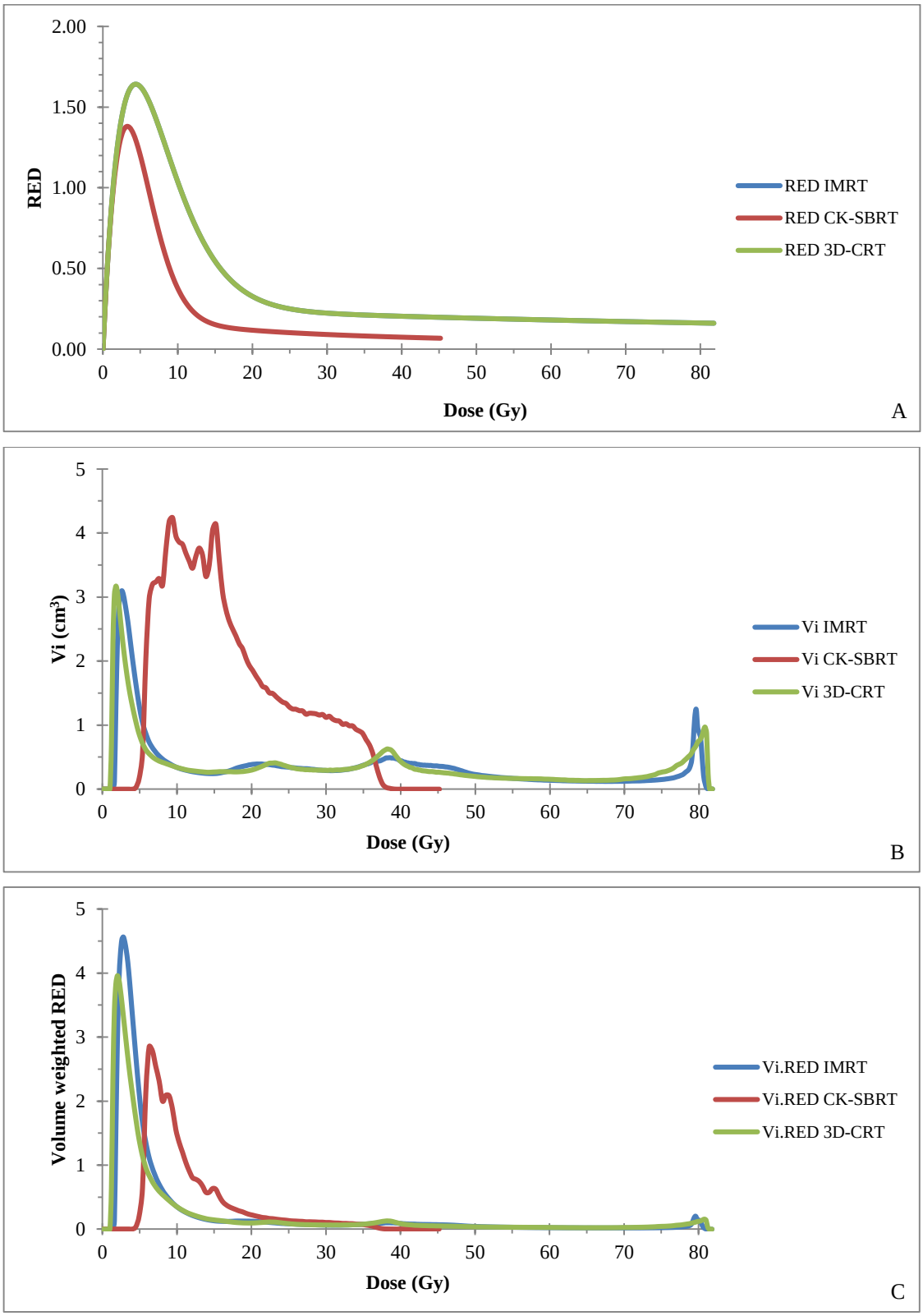

Figure 5.5 (A) Risk-equivalent dose (RED) curves, (B) Differential dose-volume histogram, (C) Volume weighted RED curves for bladder from 3D-CRT, IMRT and CK-SBRT plans

The dose-risk relationship defined by a mechanistic dose function termed as risk-equivalent dose (RED) including cell killing parameter per dose fraction and repair/repopulation during fractionated treatment allowed the assessment of effect of different dose fractionation on SPC risks. There were two types of dose-risk curves for organs involving prostate cancer treatment, i.e. bell-shaped for bladder carcinoma with large α and small R (Fig. 5.5 (A), Table 4.5) and more or less plateau curves for rectal carcinoma, pelvic bone and pelvic soft tissue sarcomas with smaller α and large R (Fig. 5.1 (A) - 5.4 (A) , Table 4.5).

Table 5.1 RED curve inflection points and doses at different volume peaks from differential dose-volume histograms. Data are doses (Gy) expressed as mean (SD).

		3D-CRT	IMRT	CK-SBRT
Pelvic soft tissue				
In-field	Curve inflection*	58.40 (5.25)	58.40 (5.25)	27.06 (2.69)
	Volume peak1	80.27 (0.63)	79.57 (0.20)	40.55 (1.00)
Near-field	Curve inflection	58.40 (5.25)	58.40 (5.25)	27.06 (2.69)
	Volume peak1	0.20 (0.13)	0.33 (0.10)	2.26 (0.41)
	Volume peak2	28.75 (2.78)	23.80 (0.90)	-
Pelvic bone	Curve inflection*	54.20 (4.82)	54.20 (4.82)	25.40 (2.51)
	Volume peak1	0.27 (0.10)	0.40 (0.18)	2.26 (0.41)
	Volume peak2	31.25 (3.25)	26.68 (1.87)	24.13 (3.79)
Rectum	Curve inflection*	37.60 (11.70)	37.60 (11.70)	15.75 (6.73)
	Volume peak1	2.53 (0.73)	3.37 (0.85)	7.23 (5.34)
	Volume peak2	-	31.97 (6.29)	21.15 (2.47)
	Volume peak3	79.40 (0.64)	79.48 (0.44)	-
Bladder	Curve inflection*	4.40 (1.64)	4.40 (1.64)	3.26 (1.38)
	Volume peak1	2.75 (0.97)	3.60 (0.89)	8.12 (2.50)
	Volume peak2	37.52 (1.15)	39.30 (2.55)	16.84 (1.82)
	Volume peak3	79.50 (0.50)	79.73 (0.16)	-

* Curve inflection is expressed in Gy.

Positive or negative dependence of SPC risk on dose was determined by the RED curve inflection point. In low dose region before the curve reached its peak, SPC risk increased with doses. Beyond its peak, SPC risk decreased either rapidly (bell-shaped curve) or slowly (plateau curve) with the increasing doses. Dose-risk curve of plateau type peaked at much greater dose than curve of bell-shaped (Table 5.1). Hypofractionation scheme used in CK-SBRT was associated with a low SPC risk in contrasting to conventional fractionation in 3D-CRT and IMRT. This was evident by the smaller area under the RED curve mainly due to a larger cell killed per dose fraction (α) and smaller cumulated dose D (Fig. 5.1 (A) - 5.5 (A)). Also, the RED curves peaked at much lower dose (Fig. 5.1 (A) - 5.5 (A), Table 5.1). This would implicate a more narrow window of SPC induction for hypofractionated treatment.

5.1.2 Influence of dose-volume histogram on RED curve

Dose-volume adjustment might result in risk enhancement or risk reduction depending on whether the volume peaked at dose before or after the RED curve inflection point. The shape of RED curves was changed after being weighted by dose-volume histogram (Fig. 5.1 -5.5 (B) and Fig. 5.1 - 5.5 (C)). For the three treatment plans optimized for the deterministic effects, major volume peaks at different doses are presented in Table 5.1. In organs with plateau type response, SPC risk at doses beyond the inflection point could be minimized by reducing the volume receiving high doses. While in the lower dose region, maintaining volume at doses far away from the inflection point would result in a better risk profile. This could be achieved for tissue with plateau-type response such as rectal carcinoma risk. At doses below the curve inflection point, 3D-CRT plan and IMRT plan had better SPC risk profiles than CK-SBRT plan because of the low dose volume peaked at doses (2.53 Gy for 3D-CRT, and 3.37 Gy for IMRT) far below the inflection point of 37.6 Gy. This was in contrast to the CK-SBRT plan where the low dose volume peaked at 7.23 Gy, much closer to the inflection point of 15.75 Gy (Table 5.1 and Fig. 5.4 (A) - 5.4 (B)).

In organ with bell-shaped curve like bladder where RED curve inflected at much lower dose level, dose-volume distribution at low dose region was of greater concern than the high dose region where cell killing played a significant role.

In this context, 3D-CRT and IMRT plans generated the low dose volume peaks respectively at doses of 2.75 Gy and 3.60 Gy which were closed to the inflection dose of 4.40 Gy where SPC reached the maximum. Alternatively, the CK-SBRT plan yielded a peak volume at 8.12 Gy which was beyond the inflection point 3.26 Gy resulting a lower SPC risk profile (Fig. 5.5 (B) – 5.5 (C)).

5.1.3 OED and EAR

Table 5.2 OEDs and EARs for organs in-field and near-field of treatment. Data are mean (SD).

Organ	3D-CRT		IMRT		CK-SBRT	
	OED (Gy)	EAR $[10^4PY]^{-1}$	OED (Gy)	EAR $[10^4PY]^{-1}$	OED (Gy)	EAR $[10^4PY]^{-1}$
Sarcoma						
- Soft tissue						
In-field	4.93	1.86	4.93	1.86	2.28	0.86
	(0.010)	(0.004)	(0.004)	(0.001)	(0.012)	(0.005)
Near-field	0.53	0.20	0.52	0.20	0.18	0.07
	(0.12)	(0.05)	(0.12)	(0.05)	(0.04)	(0.02)
- Pelvic bone	1.30	0.16	0.95	0.12	0.29	0.04
	(0.22)	(0.03)	(0.23)	(0.03)	(0.06)	(0.01)
Carcinoma						
- Rectum	8.40	2.87	8.60	2.94	5.51	1.88
	(1.10)	(0.37)	(1.12)	(0.38)	(0.57)	(0.19)
- Bladder	0.68	1.72	0.67	1.71	0.35	0.90
	(0.18)	(0.47)	(0.20)	(0.52)	(0.20)	(0.51)

RED is the risk-equivalent dose corresponding to a subvolume element of an organ receiving heterogeneous doses. The summation of weighted RED over the entire organ volume divided by V_T yielded organ equivalent dose (OED) which

was proportional to organ SPC risk and allowed the estimation of the relative risk (RR) between treatment plans.

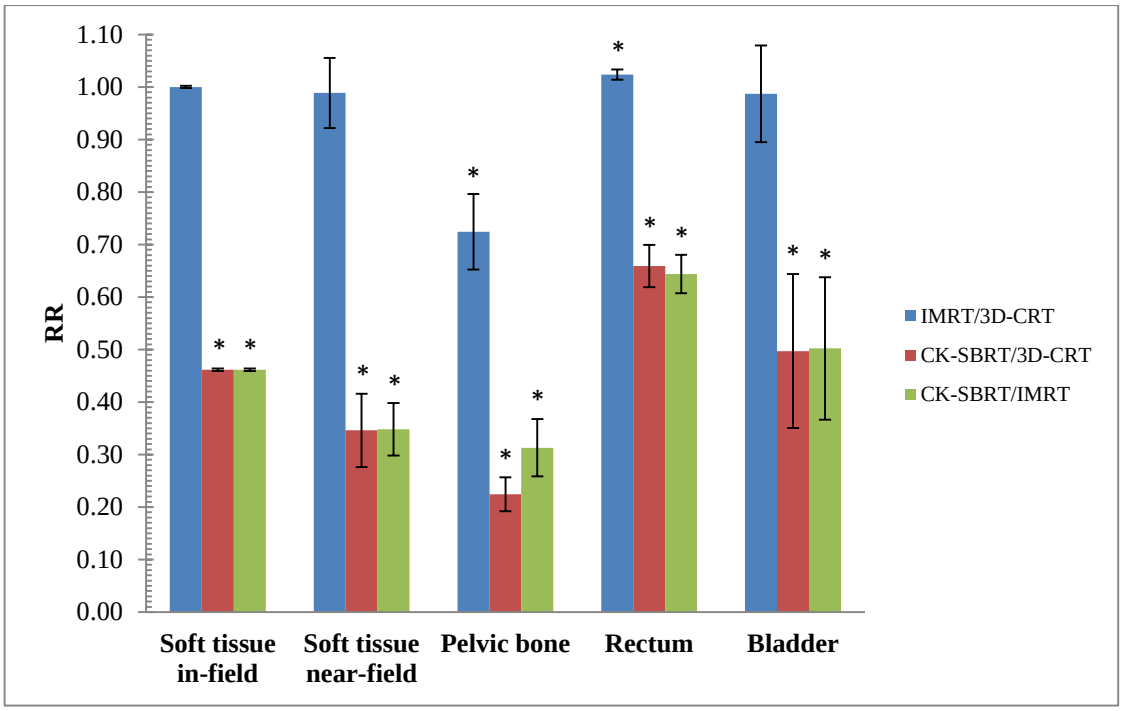

* difference with $p < 0.05$ significant

Figure 5.6 Relative risk (RR) of SPC for organs in-field and near-field of treatment relative to 3D-CRT or IMRT

With the β value and the age-dependent function for specific organ derived from atomic bomb data, the volume weighted RED, was converted to EAR (Table 5.2). Risks of SPC for organs in or near the treatment field from CK-SBRT plan were significantly less than risks from 3D-CRT and IMRT plans ($p < 0.0004$) with an average RR of 0.446 (Fig. 5.6). When comparing IMRT to 3D-CRT, an average RR of 0.99 was observed for risk of pelvic soft tissue sarcoma and bladder carcinoma. However, IMRT plan generated a significant lower risk of bone sarcoma (RR = 0.72, $p < 0.0001$) and greater risk of rectal carcinoma (RR = 1.02, $p = 0.002$). These deviations could be explained on the basis of the difference in dose-volume distribution. Regarding to bone dose-volume histogram, 3D-CRT plan generated a larger volume peak than the IMRT plan at a dose approximately half way from the inflection point, i.e. 31.25 Gy for 3D-CRT which was closer to the inflection point

of 54.20 Gy than the 26.68 Gy for IMRT. For rectum, IMRT plan created an additional volume peak near the inflection point while the 3D-CRT plan generated none (Fig. 5.4 (A) – 5.4 (B), Table 5.1).

OED did not allow the comparison of SPC risks among different organs due to the difference in organ carcinogenic susceptibility. Rectum had an OED 12-15 times greater than that of the bladder but had a β value 5 times less. After adjusting for organ-specific age modifying function, the EARs between these organs were different by a factor of 2 (Table 5.2).

5.2 SPC risks from out-of-field radiations

5.2.1 Scatter/leakage radiation as a function of distance from tumor center

Table 5.3 Scatter/leakage doses from TLDs measurement outside treatment fields for 3D-CRT, IMRT and CK-SBRT

Organ	3D-CRT			IMRT			CK-SBRT		
	Gy/MU	MU	Gy	Gy/MU	MU	Gy	Gy/MU	MU	Gy
Brain	2.19E-06	11694	0.03	2.60E-06	28379	0.07	2.48E-06	44262	0.11
Thyroid	2.44E-06	11694	0.03	2.64E-06	28379	0.07	2.96E-06	44262	0.13
Lung	2.96E-06	11694	0.03	2.63E-06	28379	0.07	2.17E-06	44262	0.10
Liver	4.70E-06	11694	0.05	4.26E-06	28379	0.12	2.26E-06	44262	0.10
Stomach	4.83E-06	11694	0.06	4.29E-06	28379	0.12	2.22E-06	44262	0.10
Kidney	1.43E-05	11694	0.17	1.31E-05	28379	0.37	3.18E-06	44262	0.14

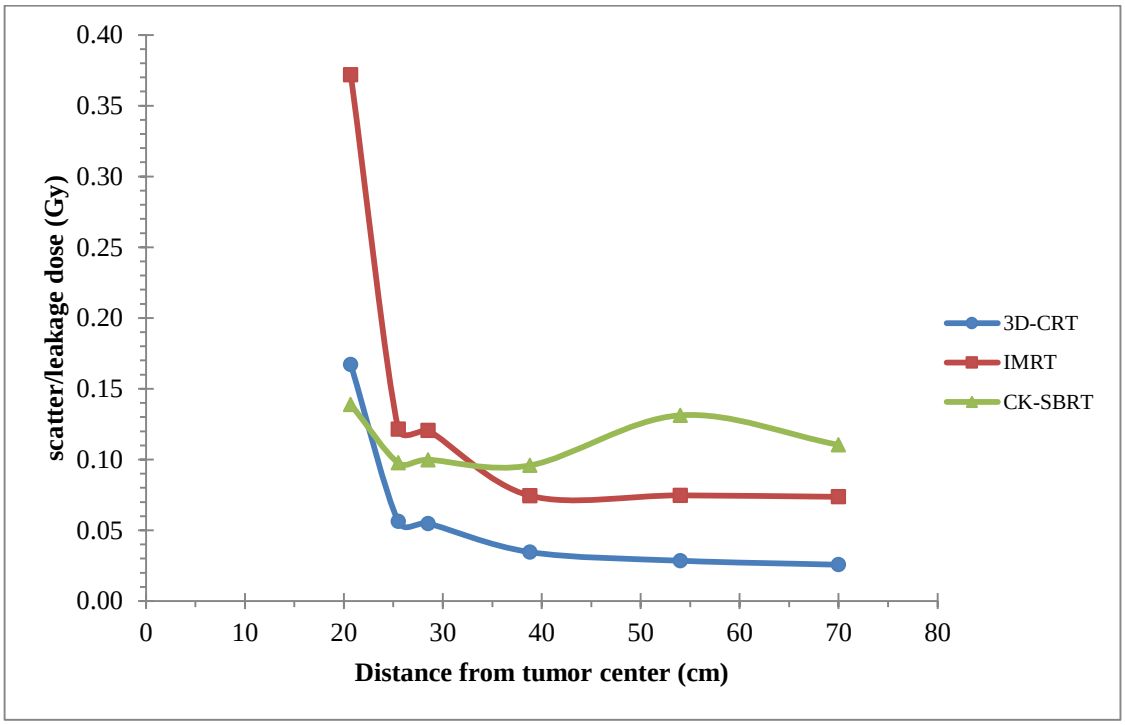

Figure 5.7 Scatter/leakage radiations as a function of distance from tumor center described for 3D-CRT, IMRT and CK-SBRT

Scatter/leakage doses as a function of distance from tumor center for 3D-CRT, IMRT and CK-SBRT are depicted in Figure 5.7. Collimator and patient scatter could be expected for 3D-CRT and IMRT plans. Since the scatter doses decreased exponentially with increasing distance from tumor center up to a distance of 40 cm. The magnitude of scatter dose from IMRT plan was approximately twice as large as compared to 3D-CRT plan. Scatter radiation from dynamic multi-leaf collimators used in IMRT could be the contributing factor since both treatment plans had comparable field sizes. For CK-SBRT, scatter radiation did not seem to be a significant contributing factor to out-of-field radiation as the scatter/leakage dose did not change with changing distance. However, CK-SBRT plan generated the largest out-of-field radiations to organs at 40 cm onward because of the greatest MU used in patient treatment.

5.2.2 Scatter/leakage doses and EARs for the out-of-field organs

Table 5.4 Scatter/leakage doses and EARs* for organs in out-of-field. Data are mean (SD).

Organ	3D-CRT		IMRT		CK-SBRT	
	D (Gy)	EAR $[10^4PY]^{-1}$	D (Gy)	EAR $[10^4PY]^{-1}$	D (Gy)	EAR $[10^4PY]^{-1}$
Brain	0.026	0.012	0.074	0.034	0.110	0.052
	(0.004)	(0.002)	(0.005)	(0.002)	(0.023)	(0.010)
Thyroid	0.029	0.003	0.075	0.008	0.131	0.014
	(0.003)	(2.80E-04)	(0.002)	(2.00E-04)	(0.021)	(0.002)
Lung	0.035	0.517	0.074	1.113	0.096	1.432
	(0.005)	(0.075)	(0.003)	(0.049)	(0.014)	(0.194)
Liver	0.055	0.113	0.121	0.249	0.100	0.206
	(0.004)	(0.009)	(0.005)	(0.011)	(0.013)	(0.024)
Stomach	0.056	0.355	0.121	0.767	0.098	0.616
	(0.004)	(0.025)	(0.007)	(0.046)	(0.013)	(0.073)
Kidney	0.167	-	0.372	-	0.139	-
	(0.009)	-	(0.030)	-	(0.012)	-

*EAR was calculated based on age x = 60 years and age a = 80 years.

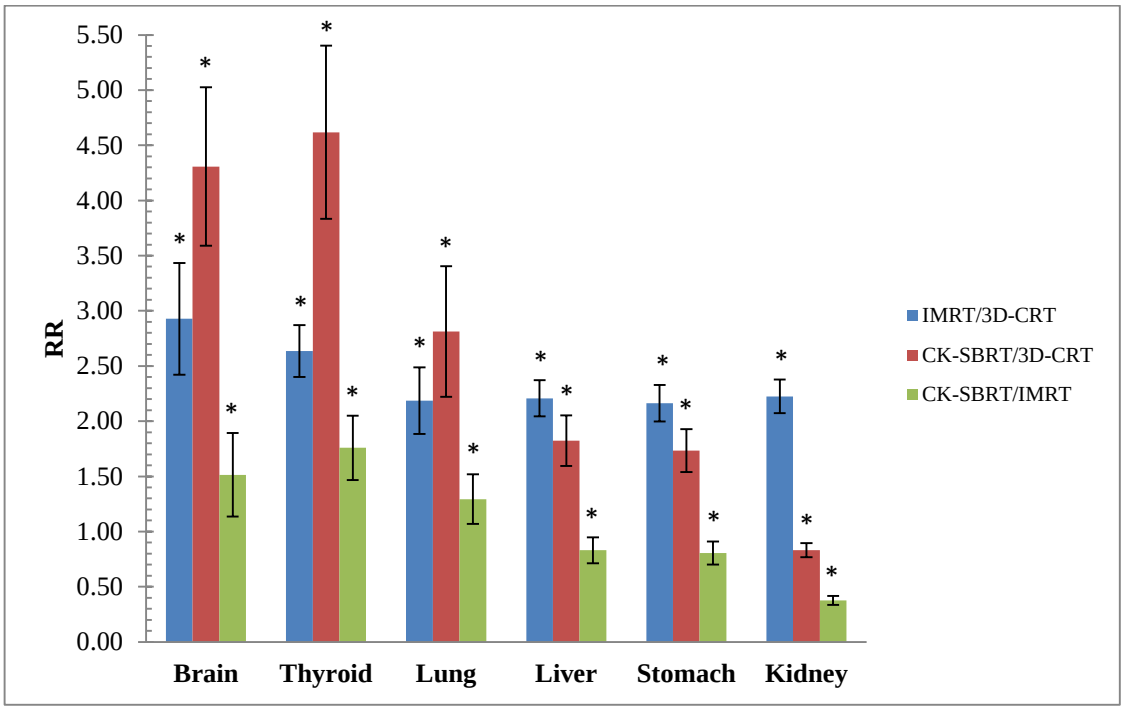

Figure 5.8 Relative risks (RR) of SPC in out-of-field organs relative to 3D-CRT or IMRT

Scatter/leakage doses and EAR for out-of-field organs determined for 3D-CRT, IMRT and CK-SBRT plans are shown in Table 5.4. Risks of SPC in out-of-field organs in relative to 3D-CRT or IMRT are shown in Figure 5.8. Risks of SPC in all out-of-field organs from IMRT plan were significantly greater than those of the 3D-CRT plan with an average RR of 2.39. For CK-SBRT plan in relative to 3D-CRT, the average RR for brain and thyroid gland were 4.46 ($p < 0.0002$). Because of the minimal patient and collimator scatters in CK-SBRT, RR was decreasing from lung (RR = 2.81, $p = 0.0002$) to kidney (RR = 0.83, $p = 0.0012$). CK-SBRT in comparing to IMRT, RRs were slightly but significantly greater than 1 for brain, thyroid gland, and lung. However, the treatment was less carcinogenic for organs like liver, stomach and kidney with RRs of 0.83, 0.81 and 0.38, respectively, $p < 0.02$.

Scatter/leakage dose was not an absolute estimate for SPC risk when different organs came into question. Taking the organ-specific β and age-modifying function into consideration, brain, thyroid and lung although received comparable doses but the EARs were largest for lung followed by brain and thyroid (Table 5.4).

5.3 SPC risks from image-guided procedures

5.3.1 Doses from image-guided procedures used in 3D-CRT, IMRT and CK-SBRT.

Doses from image-guided procedures used in 3D-CRT, IMRT and CK-SBRT are showed in Tables 5.5-5.7.

Table 5.5 Imaging doses from the image-guided protocol used in 3D-CRT. Data are mean (SD).

Organ	Shape of treatment field		Patient position		Total dose
	Gy/image	Gy/procedure	Gy/image	Gy/procedure	Gy/protocol
Prostate	0.007	0.050	0.007	0.110	0.160
	(1.55E-04)	(1.09E-03)	(1.06E-04)	(1.69E-03)	(2.73E-03)
Rectum	0.005	0.033	0.005	0.075	0.109
	(9.37E-05)	(6.56E-04)	(3.28E-04)	(5.25E-03)	(4.60E-03)
Bladder	0.006	0.041	0.006	0.089	0.129
	(2.83E-04)	(1.98E-03)	(1.82E-04)	(2.92E-03)	(4.86E-03)
Liver	3.24E-05	2.27E-04	3.64E-05	5.83E-04	8.09E-04
	(9.90E-07)	(6.93E-06)	(1.01E-06)	(1.61E-05)	(2.26E-05)
Stomach	3.26E-05	2.28E-04	3.79E-05	6.06E-04	8.34E-04
	(5.57E-07)	(3.90E-06)	(6.23E-07)	(9.97E-06)	(1.15E-05)
Kidney	8.91E-05	6.24E-04	9.36E-05	1.50E-03	2.12E-03
	(2.52E-06)	(1.76E-05)	(5.90E-07)	(9.44E-06)	(2.24E-05)

Table 5.6 Imaging doses from the image-guided protocol used in IMRT. Data are mean (SD).

Organ	CBCT		AP		LAT		Total dose
	Gy / image	Gy / procedure	Gy / image	Gy / procedure	Gy / image	Gy / procedure	Gy / protocol
Prostate	0.022 (4.07E-04)	0.222 (0.004)	2.36E-04 (1.60E-05)	0.009 (6.08E-04)	7.52E-04 (5.43E-05)	0.029 (0.002)	0.259 (0.006)
Rectum	0.019 (4.75E-04)	0.189 (0.005)	7.76E-05 (5.60E-06)	0.003 (2.13E-04)	8.10E-04 (4.57E-05)	0.031 (0.002)	0.222 (0.007)
Bladder	0.023 (4.32E-04)	0.232 (0.004)	3.79E-04 (2.70E-05)	0.014 (1.03E-03)	7.18E-04 (3.68E-05)	0.027 (0.001)	0.274 (0.007)
Liver	0.001 (9.84E-06)	0.007 (9.84E-05)	4.02E-06 (3.82E-08)	1.53E-04 (1.45E-06)	5.06E-05 (3.45E-06)	0.002 (1.31E-04)	0.009 (1.85E-04)
Stomach	0.001 (1.62E-05)	0.006 (1.62E-04)	4.22E-06 (1.49E-07)	1.61E-04 (5.66E-06)	2.00E-05 (1.35E-06)	0.001 (5.13E-05)	0.007 (1.76E-04)
Kidney	0.002 (3.83E-05)	0.018 (3.83E-04)	8.65E-06 (5.62E-08)	3.29E-04 (2.14E-06)	1.03E-04 (7.43E-06)	0.004 (2.83E-04)	0.023 (6.12E-04)

Table 5.7 Imaging doses from the image-guided protocol used in CK-SBRT. Data are mean (SD).

Organ	Tumor tracking	
	Dose (Gy) / image	Dose (Gy) / whole course
Prostate	1.52E-04	0.170
	(2.67E-05)	(0.022)
Rectum	8.13E-05	0.091
	(1.11E-05)	(0.012)
Bladder	2.91E-04	0.326
	(2.66E-05)	(0.043)
Liver	1.09E-05	0.012
	(1.83E-06)	(0.002)
Stomach	1.19E-05	0.013
	(9.17E-07)	(0.002)
Kidney	4.94E-05	0.055
	(8.10E-06)	(0.007)

The mean number of images were 1122 images (range 880 – 1275 images).

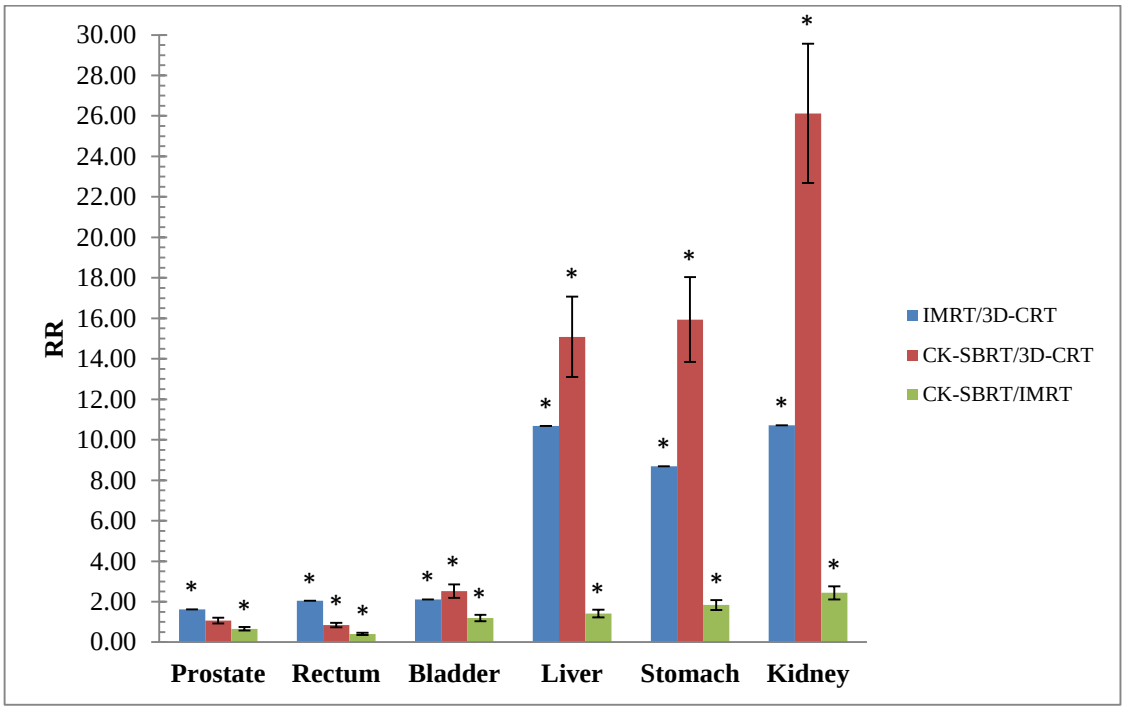

Figure 5.9 Relative risks (RR) of SPC for imaging dose relative to 3D-CRT or IMRT

Image-guided procedures involved many organs including prostate, bladder, rectum, kidney, liver and stomach. The field of views were 20 x 26 cm^2 for 3D-CRT and IMRT and 59 x 66 cm^2 for CK-SBRT. Total number of images were 23 for 3D-CRT, 86 for IMRT and 1122 (880 – 1275) for CK-SBRT. Details of image-guided doses to organs involved are summarized in Tables 5.5 – 5.7. The RRs for prostate, rectum and bladder between treatment plans were comparable but mostly significant difference. SPC risks for liver, stomach and kidney from procedures used in CK-SBRT and IMRT were at least 10 folds greater than those of the 3D-CRT. While the risks between CK-SBRT and IMRT were comparable but significantly larger for CK-SBRT (Fig. 5.9).

5.3.2 EAR for organs involving image-guided exposure

Table 5.8 EARs for organs receiving doses from image-guided procedures used in 3D-CRT, IMRT and CK-SBRT. Data are mean (SD).

Organ	3D-CRT		IMRT		CK-SBRT	
	Dose (Gy)	EAR $[10^{-4}PY]^{-1}$	Dose (Gy)	EAR $[10^{-4}PY]^{-1}$	Dose (Gy)	EAR $[10^{-4}PY]^{-1}$
Prostate	0.160	0.060	0.259	0.098	0.170	0.064
	(2.73E-03)	(0.000)	(0.006)	(0.000)	(0.022)	(0.008)
Rectum	0.109	0.037	0.222	0.076	0.091	0.031
	(4.60E-03)	(0.000)	(0.007)	(0.000)	(0.012)	(0.004)
Bladder	0.129	0.329	0.274	0.696	0.326	0.829
	(4.86E-03)	(0.000)	(0.007)	(0.000)	(0.043)	(0.109)
Liver	8.09E-04	0.002	0.009	0.018	0.012	0.025
	(2.26E-05)	(0.000)	(1.85E-04)	(0.000)	(0.002)	(0.003)
Stomach	8.34E-04	0.005	0.007	0.046	0.013	0.084
	(1.15E-05)	(0.000)	(1.76E-04)	(0.000)	(0.002)	(0.011)
Kidney	0.002	-	0.023	-	0.055	-
	(2.24E-05)	-	(6.12E-04)	-	(0.007)	-

EARs for organs receiving image-guided doses were calculated and are presented in Table 5.8. At the prostate location, EAR was determined for sarcoma risk expected for the tumor bed using pelvic soft tissue data. EAR for kidney was omitted because of the lack of cancer induction parameter [22]. Bladder had the largest EAR due to higher carcinogenic susceptibility (β) and also due to large imaging dose as observed for CK-SBRT protocol.

5.4 Total SPC risks for 3D-CRT, IMRT and CK-SBRT.

For different sources of carcinogenic doses, i.e. primary beam component (in or near-field), scatter/leakage radiation and image-guided procedure, EARs from different organ sites were pooled and that EAR from the total procedures for each patient was calculated (Tables 5.9 – 5.11).

Table 5.9 EARs for 3D-CRT from primary beam component, scatter/leakage radiation and image-guided procedures

	EAR for 3D-CRT $[10^{-4}PY]^{-1}$			
	EAR_{prim}	**EAR_{scatt}**	**EAR_{image}**	**EAR_{total}**
Pt.1	6.784	1.075	0.433	8.292
Pt.2	6.540	0.924	0.433	7.898
Pt.3	6.921	0.948	0.433	8.302
Pt.4	6.269	0.955	0.433	7.657
Pt.5	7.312	0.955	0.433	8.700
Pt.6	7.066	1.151	0.433	8.650
Mean	6.815	1.001	0.433	8.250
SD	0.373	0.090	0.000	0.410

Table 5.10 EARs for IMRT from primary beam component, scatter/leakage radiation and image-guided procedures

	EAR for IMRT $[10^{-4}PY]^{-1}$			
	EAR_{prim}	**EAR_{scatt}**	**EAR_{image}**	**EAR_{total}**
Pt.1	6.695	2.257	0.934	9.885
Pt.2	6.608	2.144	0.934	9.686
Pt.3	6.871	2.066	0.934	9.872
Pt.4	6.428	2.298	0.934	9.660
Pt.5	7.126	2.210	0.934	10.270
Pt.6	7.197	2.052	0.934	10.183
Mean	6.821	2.171	0.934	9.926
SD	0.301	0.101	0.000	0.252

Table 5.11 EARs for CK-SBRT from primary beam component, scatter/leakage radiation and image-guided procedures

	EAR for CK-SBRT $[10^{-4}PY]^{-1}$			
	EAR_{prim}	**EAR_{scatt}**	**EAR_{image}**	**EAR_{total}**
Pt.1	3.451	2.313	1.175	6.940
Pt.2	3.415	2.670	1.125	7.210
Pt.3	3.882	2.035	0.936	6.853
Pt.4	3.344	1.844	1.102	6.290
Pt.5	3.940	2.595	1.056	7.590
Pt.6	4.452	2.467	0.811	7.730
Mean	3.747	2.321	1.034	7.102
SD	0.427	0.325	0.136	0.528

Table 5.12 EAR_{total} for 3D-CRT, IMRT and CK-SBRT

	EAR_{total} $[10^{-4}PY]^{-1}$		
	3D-CRT	**IMRT**	**CK-SBRT**
Pt.1	8.292	9.885	6.940
Pt.2	7.898	9.686	7.210
Pt.3	8.302	9.872	6.853
Pt.4	7.657	9.660	6.290
Pt.5	8.700	10.270	7.590
Pt.6	8.650	10.183	7.730
Mean	8.250	9.926	7.102
SD	0.410	0.252	0.528

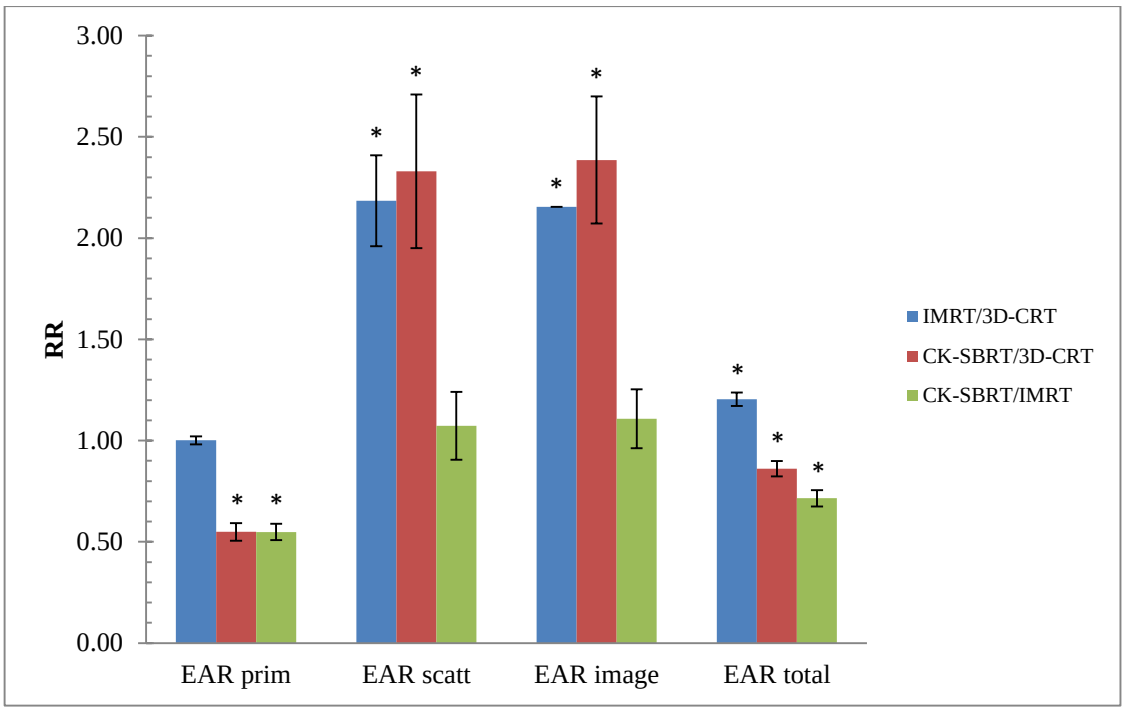

Figure 5.10 Relative risks (RR) of SPC for EAR_{prim}, EAR_{scatt} and EAR_{image} relative to 3D-CRT or IMRT

3D-CRT and IMRT generated comparable EARs ($p = 0.922$) for organs in or near treatment field but these EARs were nearly twice as large as that for the CK-SBRT plan. Image-guided procedures further added a small fraction of SPC risks to organ in or near treatment field. EARs from image-guided procedure used in IMRT and CK-SBRT were comparable ($p = 0.131$) but were 2.3 folds larger than that of 3D-CRT ($p = 0.0001$). Similar trend was observed for scatter/leakage component. Combining the EARs from all sources of carcinogenic doses yielded EARs of 8.25, 9.93 and 7.10 excess cases per 10^4 PY for 3D-CRT, IMRT and CK-SBRT, respectively. All estimations differed significantly ($p < 0.0002$).

CHAPTER VI
DICUSSION

Radiation-induced second primary cancer (SPC) in normal tissues is the late treatment complication of great concern in successful cancer treatment. Approaches to mitigate risk of SPC have become an increasingly important subject in clinical radiation oncology. Areas of radiation research suggesting strong evidence toward SPC risk are genetic factor, patient age at the time of radiotherapy, tissue sites receiving irradiation and the dose-volume relationship for organs in the vicinity of the treatment field [52]. Type of dose fractionation may have an impact on SPC induction. Schneider et al [53] had demonstrated by mathematical model prediction that hypofractionated radiotherapy might have a potential in SPC reduction.

Modern RT technologies have greatly reduced the volume of normal tissue receiving high doses thereby lower the acute and late tissue toxicities and possibly SPC risk [52]. Nevertheless, whether the newer conformal RT technologies will necessarily reduce the risk of SPC is a subject of continued debate. The idea of better dose targeting in reduction of SPC risk has been challenged by the concern of image volume of normal tissues being exposed to low radiation doses which are mutagenic prone rather than cytotoxic as expected in high doses. Modern RT technologies also involve longer beam on time resulting increased scatter/leakage doses. The use of image-guided procedures to ensure precise tumor dose delivery further adds extra doses to the patient.

In this study, we used the well-accepted cancer induction model developed by Schneider et al [53] to demonstrate that type of dose fractionation and dose-volume relationship played the significant part in SPC induction for tissues located in or closed to the treatment fields. According to the model calculations, there was two types of dose-risk curves i.e. bell-shaped for bladder and more or less plateau curve for rectum, bone, and soft tissue sarcomas. The curve inflection point would determine whether the SPC risk increased or decreased with increasing doses. At the low dose

region, before the curve reached its peak, SPC risk increased with dose. Beyond its peak, SPC risk rapidly (bell-shaped) or slowly (plateau) decreased with increasing doses.

Adjusting the dose-volume distribution is a means to weigh-in or weigh-out the SPC risk. Large volume to doses far below the inflection point would weigh-out SPC risk while volume distributed near the curve inflection would weigh-in the risk. Beyond the inflection point, reducing volume receiving high doses would greatly lower the SPC risks particularly for tissues with plateau type of response like rectum, bone and soft tissue sarcomas. This was in contrast to bladder with a bell-shaped curve. High doses were more cytotoxic than carcinogenic. The large volume of bladder exposed to high doses would be related to late deterministic complications, not the late stochastic risks.

The SPC induction model incorporated linear-quadratic function to an account of dose fractionation effect and also the repair/repopulation factor to allow the conversion of physical dose (D) into a risk equivalent dose (RED). This formulation allowed the comparative analysis of RED between conventional dose fractionation used in 3D-CRT and IMRT with the hypofractionation used in CK-SBRT. Biologically effective ablative dose fractions in hypofractionation regime induced equivalent treatment effect at lower dose. As a consequence, greater cell killed per dose fraction and the lower cumulated dose to normal tissue in the hypofractionated treatment resulted in a lower SPC risk as evidenced by a smaller area under RED curve and a lower inflection point.

Taken all these together, we might suggest that large volume of tissue exposed to low doses either leading to SPC risk elevation or reduction depending on type of dose-risk response and type of dose-fractionation. This notion was supported the observation in rectum response at low dose region. Lower SPC risk profiles were noted in 3D-CRT and IMRT plans because the volume peaks locating at dose levels far away from the RED curve inflection point. For CK-SBRT plan, a greater risk profile was observed as the volume peaked around the curve inflection which was related to the high-risk level. However, the situation was reversed for bladder with a bell-shaped curve. Lower SPC risk was observed for CK-SBRT as the volume peaked beyond the inflection point of the descending limb of the RED curve while risk

profiles for 3D-CRT and IMRT were greater since the volume peaked near the curve inflection.

Excess absolute risk (EAR) calculated for a certain value of RED represented the risk of a small volume element of an organ. The summation of fractional volume weighted EAR over the total organ yielded an EAR^{org} which was comparable to those reported in literature. EAR^{org} was proportion to organ equivalent dose (OED). Magnitude of OED for organ in-field (i.e. tumor bed) and near-field (pelvic soft tissue, bone, bladder and rectum) was proportional to area under the dose-risk curve which was dictated by shape of dose risk curve, type of dose-fractionation and dose-volume histogram. For instance, 3D-CRT and IMRT plans which had similar dose fractionation and dose-volume distribution, OED for rectum with a plateau type of response were larger than that of bladder with a bell-shaped response. However, the magnitude of EAR^{org} was not only determined by OED but also by the organ carcinogenic susceptibility. Based on the A-bomb data on cancer risk, rectum was less susceptible to carcinogenesis with a β value of 0.73 per 10^4 PYGy which was lower than the β (3.8 per 10^4 PYGy) for bladder. On this basis EAR estimates for rectum and bladder were comparable. If was quite interesting to obtain also a comparable EAR for lung which located distantly from the treatment field and received only low dose of scatter/leakage radiation. A large value of β for lung, 8 per 10^4 PYGy, could be the significant contributing factor. Nevertheless, the model predictions were in good agreement with the finding by Brenner et al [18].

With comparable dose-volume histograms between 3D-CRT and IMRT plans, no difference in SPC risks was confirmed for these modalities with an average relative risk (RR) of 0.99. When either the 3D-CRT or IMRT plan was compared to that of CK-SBRT, SPC risks for organs in or near the CK-SBRT treatment field were significantly reduced by at least 45% with an average RR of 0.55. Similar findings using the same risk model were reported by Murray et al [17] although they used a slightly different hypofractionated scheme i.e. 7 fractions of 6.1 Gy in contrast the 5 fractions of 7.25 Gy for this study. Combining the EARs from all organ sites, the overall excess cases of SPC per 10^4 PY were 6.82 for 3D-CRT, and IMRT and 3.75 CK-SBRT. Image-guided procedures used by these modalities further added a small fraction of SPC to organs in or near the treatment fields. The image-guided

protocol associated EARs were 0.43, 0.93 and 1.03 per 10^4 PY for 3D-CRT, IMRT and CK-SBRT, respectively.

Increased scatter/leakage radiations in modern conformal RT has long been the concern for the elevation of SPC risk [54]. In this study, we observed CK-SBRT generated the greatest scatter/leakage radiation due to the use of largest MU units. While IMRT and 3D-CRT generated lower levels of scatter/leakage radiations but higher patient scatter to organs near the field edge including kidney, stomach and liver. Although the MU used in CK-SBRT was twice as large as that for IMRT, minimal patient scatter helped to compensate the SPC risk. In overall, EARs from these two modalities were comparable, i.e. 2.17 and 2.32 excess cases per 10^4 PY for IMRT and CK-SBRT, respectively. EAR from scatter/leakage radiation for 3D-CRT was 1 excess cases per 10^4 PY.

Combining SPC risks from all sources yielded comparable overall EARs for this contemporary RT, i.e. 9.93 and 7.10 excess cases per 10^4 PY for IMRT and CK-SBRT, in contrasting to 8.25 excess cases per 10^4 PY for 3D-CRT. How were these findings compared to other studies. Comparing these EAR estimates to epidemiological finding would be difficult since most studies quantified the SPC risk without providing any details about the confounding factors such as age, race, smoking, etc. However, Murray et al [17] suggested the SPC rate in the order of 3 to 5 per 1000. In one study by Liauw et al [54], a relative risk of 2.34 was reported for secondary bladder cancer after prostate radiotherapy, compared to general population. This relative risk remained unchanged over increasing follow-up intervals up to 20 years and was equivalent to an EAR of 35 per 10^4 PY. Our EAR estimates were much lower and all treatments used modern conformal RT technologies in contrasting to the old technique of 2D-RT reported by Liauw et al [54]. In fact, trends in SPC reduction by 3D-CRT and IMRT were addressed previously [19, 20]. Regarding to the stereotactic technology, an institutional study on risk of SPC after gamma knife stereotactic radiosurgery in approximately 5,000 patients and 30,000 patient-years of follow-up, the authors reported only a new astrocytoma 8 years after the treatment. This was lower than the 2.47 cases predicted based on national incidence figures [55]. No increased risk of SPC was concluded. Lately, Berrington de Gonzalez et al [56] screened prostate cancer patients in the Surveillance Epidemiology and End Results

(SEER)-Medicare data base from 1992 to 2004, who were 66-84 years at diagnosis, treated by 2D-RT, 3D-CRT and brachytherapy. The patients were followed through 2009. Analyzes of second solid cancers were based on 38,733 5-year survivors and second leukemia on 52,515 2-year survivors. They found no significant differences in overall second solid cancers between 2D-RT and 3D-CRT patients, but the second rectal cancer rates were significantly lower after 3D-CRT. Significant reductions in colon cancer and leukemia rates were observed in the first decade after brachytherapy compared to those after external beam RT.

CHAPTER VII
CONCLUSION

7.1 SPC risks for organs in or near treatment fields

7.1.1 Based on the risk-equivalent dose (RED) model, hypofractionation using a few ablative dose fractions and lower treatment dose generated lower SPC risks to organs in or near the treatment fields than the conventional fractionation.

7.1.2 Dose volume adjustment to allow large volume of tissues irradiated to doses far below the RED curve inflection could greatly reduce the SPC risk. Doses closed to the curve inflection were associated with a high SPC risk.

7.1.3 EAR^{org} of an organ was a function of organ-specific carcinogenic susceptibility and OED which was dependent on the shape of dose-risk curve (bell-shaped or plateau), dose fractionation and organ dose-volume histogram.

7.1.4 Because of the similarity in dose-volume histograms for 3D-CRT and IMRT plans, SPC risks for organs in or near the treatment fields were more or less the same except for rectum where IMRT generated a greater risk with an RR of 1.02 due to the presence of an additional volume peak near the inflection point. The opposite was true for the pelvic bone sarcoma where 3D-CRT plan created a greater risk owing to the low dose volume peaked at a dose closer to the curve inflection than the IMRT plan.

7.1.5 Risks of SPC for all organs in or near the treatment fields of CK-SBRT were less than the risks from 3D-CRT and IMRT with an average RR of 0.446.

7.2 SPC risks in out-of-field organs

7.2.1 For organs distal to the field edge like thyroid and brain, CK-SBRT and IMRT in relative to 3D-CRT generated an average RR of 4.46 and 2.78 for CK-SBRT and IMRT, respectively.

7.2.2 Because of the minimal patient scatter in CK-SBRT, organs at the intermediate distance from the field edge like lung, liver, stomach and kidneys, the RR for CK-SBRT in relative to 3D-CRT were decreasing from lung (RR = 2.81) to kidneys (RR= 0.83)

7.3 SPC risks from image-guided procedures

7.3.1 Image-guided procedures contributed much less radiation doses to organs in or near the treatment fields and also those organs receiving scatter/leakage radiations.

7.3.2 Among treatment comparisons, the RRs for prostate site, rectum and bladder were approximately 2 fold greater than 3D-CRT procedure. While in organs including liver, stomach and kidneys, the RRs for CK-SBRT or IMRT were at least 10 folds larger.

7.4. Total EAR for the primary beam component, scatter/leakage radiation and image-guided procedure

7.4.1 3D-CRT and IMRT generated comparable EARs for organs in or near the treatment fields and these EARs were nearly twice as large as that for CK-SBRT plan.

7.4.2 Image-guided procedures further added a small fraction of SPC risks to organs in or near the treatment fields as well the out-of-field organs. EARs from image-guided procedures used in IMRT and CK-SBRT were comparable but were 2.3 folds larger than the 3D-CRT procedure.

7.4.3 A similar trend was observed for scatter/leakage radiation.

7.4.4 Combining the EARs from all sources of carcinogenic doses yielded EARs of 8.25, 9.93 and 7.10 excess cases per 10^4 PY for 3D-CRT, IMRT, and CK-SBRT, respectively.

REFFERENCES

1. Jemal A, Bray F, Melissa M. Center, Ferlay J, Ward E, Forman D. Global cancer statistics. CA CANCER J CLIN. 2011;61(2):69-90.
2. Haas GP, Delongchamps N, Brawley OW, Wang CY, Gustavo de la Roza. The worldwide epidemiology of prostate cancer: perspectives from autopsy studies. Can J Urol. 2008;15(1):3866–71.
3. Shao YH, Demissie K, Shih W, Mehta AR, Stein MN, Roberts CB, et al. Contemporary risk profile of prostate cancer in the United States. J Natl Cancer Inst. 2009;101(18):1280-3.
4. Mohan R, Schellhammer PF. Treatment options for localized prostate cancer. Am Fam Physician. 2011;84(4):413-20.
5. Graham J, Baker M, Macbeth F, Titshall V. Diagnosis and treatment of prostate cancer: summary of NICE guidance. BMJ. 2008;336:610-2.
6. Bechis SK, Carroll PR, Cooperberg MR. Impact of age at diagnosis on prostate cancer treatment and survival. J Clin Oncol. 2011;29(2):235-41.
7. Welch HG, Albertsen PC. Prostate cancer diagnosis and treatment after the introduction of prostate-specific antigen screening: 1986-2005. J Natl Cancer Inst. 2009;101:1325-9.
8. Critz FA, Levinson K. 10-year disease-free survival rates after simultaneous irradiation for prostate cancer with a focus on calculation methodology. J Urol. 2004;172:2232-8.
9. Krygiel JM, Smith DS, Homan SM, Sumner W, Nease RF, Brownson RC, et al. Intermediate term biochemical progression rates after radical prostatectomy and radiotherapy in patients with screen detected prostate cancer. J Urol. 2005;174(1):126-30.

10. Stephenson AJ, Scardino PT, Eastham JA, Bianco FJ, Dotan ZA, Diblasio CJ, et al. Postoperative nomogram predicting the 10-year probability of prostate cancer recurrence after radical prostatectomy. J Clin Oncol. 2005;23(28):7005–12.
11. Martin NE, D'Amico AV. Progress and controversies: Radiation therapy for prostate cancer. CA CANCER J CLIN. 2014;64(6):389-407.
12. Dasu A, Toma-Dasu I. Prostate alpha/beta revisited - an analysis of clinical results from 14,168 patients. Acta Oncol. 2012;51(8):963-74.
13. Miralbell R, Roberts SA, Zubizarreta E, Hendry JH. Dose-fractionation sensitivity of prostate cancer deduced from radiotherapy outcomes of 5,969 patients in seven international institutional datasets: α/β = 1.4 (0.9-2.2) Gy. Int J Radiat Oncol Biol Phys. 2012;82(1):17-24.
14. Katz AJ, Santoro M, Diblasio F, Ashley R. Stereotactic body radiotherapy for localized prostate cancer: disease control and quality of life at 6 years. Radiation Oncology. 2013;8(118):1-8.
15. Davis EJ, Beebe-Dimmer JL, Yee CL, Cooney KA. Risk of second primary tumors in men diagnosed with prostate cancer: a population-based cohort study. Cancer. 2014;120(17):2735-41.
16. Braunstein S, Nakamura JL. Radiotherapy-induced malignancies: review of clinical features, pathobiology, and evolving approaches for mitigating risk. Front Oncol. 2013;3(73):1-15.
17. Murray L, Thompson MC, Lilley J, Cosgrove V, Franks K, Sebag-Montefiore D, et al. Radiation-induced second primary cancer risks from modern external beam radiotherapy for early prostate cancer: impact of stereotactic ablative radiotherapy (SABR), volumetric modulated arc therapy (VMAT) and flattening filter free (FFF) radiotherapy. Phys. Med. Biol. 2015;60:1237-57.
18. Brenner DJ, Curtis RE, Hall EJ, Ron E. Second malignancies in prostate carcinoma patients after radiotherapy compared with surgery. Cancer. 2000;88:398–406.

19. Huang J, Kestin LL, Ye H, Wallace M, Martinez AA, Vicini FA. Analysis of second malignancies after modern radiotherapy versus prostatectomy for localized prostate cancer. Radiotherapy and oncology. 2011;98(1):81-6.
20. Zelefsky MJ, Pei X, Teslova T, Kuk D, Magsanoc JM, Kollmeier M, et al. Secondary cancers after intensity-modulated radiotherapy, brachytherapy and radical prostatectomy for the treatment of prostate cancer: incidence and cause-specific survival outcomes according to the initial treatment intervention. BJU Int. 2012;110(11):1696-701.
21. Schneider U. Mechanistic model of radiation-induced cancer after fractionated radiotherapy using the linear-quadratic formula. Medical physics. 2009;36(4):1138-43.
22. Schneider U, Sumila M, Robotka J. Site-specific dose-response relationships for cancer induction from the combined Japanese A-bomb and Hodgkin cohorts for doses relevant to radiotherapy. Theoretical biology and medical modelling. 2011;8(27):1-21.
23. Berrington de Gonzalez A, Gilbert E, Curtis R, Inskip P, Kleinerman R, Morton L, et al. Second solid cancers after radiation therapy: a systematic review of the epidemiologic studies of the radiation dose-response relationship. Int J Radiat Oncol Biol Phys. 2013;86(2):224-33.
24. Hall EJ, Wuu CS. Radiation-induced second cancers: the impact of 3D-CRT and IMRT. Int J Radiat Oncol Biol Phys. 2003;56(1):83-8.
25. Dörr W, Herrmann T. Second primary tumors after radiotherapy for malignancies. Strahlenther Onkol. 2002;178(7):357-62.
26. Sasse S, Klimm B, Gorgen H, Fuchs M, Heyden-Honerkamp A, Lohri A, et al. Comparing long-term toxicity and efficacy of combined modality treatment including extended- or involved-field radiotherapy in early-stage Hodgkin's lymphoma. Annals of oncology. 2012;23(11):2953-9.
27. Deng J, Zhang Y, Zhou L, Ming X, Zhang Y, Wu H, et al. Why are we concerned about imaging dose in the radiotherapy of cancers. Austin J Radiol. 2014;1(1):1-3.
28. National research council. Health risks from exposure to low levels of ionizing radiation BEIR VII Phase 2. The National Academies Press. 2006.

29. Neugut AI, Ahsan H, Robinson E, Ennis R. Bladder carcinoma and other second malignancies after radiotherapy for prostate carcinoma. Cancer. 1997;79:1600-4.
30. Diallo I, Haddy N, Adjadj E, Samand A, Quiniou E, Chavaudra J, et al. Frequency distribution of second solid cancer locations in relation to the irradiated volume among 115 patients treated for childhood cancer. Int J Radiat Oncol Biol Phys. 2009;74(3):876-83.
31. Brenner DJ, Hall EJ. Secondary neutrons in clinical proton radiotherapy: a charged issue. Radiotherapy and oncology. 2008;86(2):165-70.
32. Doss M. Linear No-Threshold model VS. radiation hormesis. Dose-response. 2013;11:480-97.
33. Hall EJ, Phil D. Intensity-modulated radiation therapy, protons, and the risk of second cancers. Int J Radiation Oncology Biol Phys. 2006;65(1):1-7.
34. Gray LH. Cellualr Radiation Biology: A symposium considering radiation effects in the cell and possible implications for cancer therapy. Radiation biology and cancer. 1965:7-25.
35. Spiess H, Mays CW. Bone cancers induced by 224 Ra (Th X) in children and adults. Health Phys. 1970;19(6):713-29.
36. Sigurdson AJ, Ronckers CM, Mertens AC, Stovall M, Smith SA, Liu Y, et al. Primary thyroid cancer after a first tumour in childhood (the childhood cancer survivor study): a nested case-control study. The Lancet. 2005;365(9476):2014-23.
37. Dörr W, Herrmann T. Cancer induction by radiotherapy: dose dependence and spatial relationship to irradiated volume. Radiol Prot. 2002;22(3A).
38. Schneider U, Kaser-Hotz B. Radiation risk estimates after radiotherapy: application of the organ equivalent dose concept to plateau dose-response relationships. Radiat Environ Biophys. 2005;44(3):235-9.
39. Schneider U, Zwahlen D, Ross D, Kaser-Hotz B. Estimation of radiation-induced cancer from three-dimensional dose distributions: Concept of organ equivalent dose. Int J Radiation Oncology Biol Phys. 2005;61(5):1510-5.

40. Kan MW, Leung LH, Wong W, Lam N. Radiation dose from cone beam computed tomography for image-guided radiation therapy. Int J Radiation Oncology Biol Phys. 2008;70(1):272-9.
41. Varian Medical Systems Inc. Varian Clinac iX specifications. 2005:1-16.
42. Pantelis E, Petrokokkinos L, Antypas C. Image guidance quality assurance of a G4 CyberKnife robotic stereotactic radiosurgery system. JINST. 2009;4(05):1-7.
43. Thermolumimescent dosimetry material. Available at: http://www.thermoscientific.com.
44. Dong S.L., Chu T.C., Lan G.Y., Wu T.H., Lin Y.C., Lee J.S. Characterization of high-sensitivity metal oxide semiconductor field effect transistor dosimeters system and LiF:Mg,Cu,P thermoluminescence dosimeters for use in diagnostic radiology. Applied Radiation and Isotopes. 2002;57:883-91.
45. Mércia Liane de Oliveira, Maia AF, Natália Cássia do Espírito Santo Nascimento, Maria da Conceição de Farias Fragoso, Galindo RS, Hazin CA. Influence of thermoluminescent dosimeters energy dependence on the measurement of entrance skin dose in radiographic procedures. Radiol Bras. 2010;43(2):113-8.
46. The Alderson radiation therapy phantom (ART). Available at: http://www.rsdphantoms.com.
47. Radiation Therapy Oncology Group. A phase III randomized study of hypofractionated 3D-CRT/IMRT versus conventionally fractionated 3D-CRT/IMRT in patients with favorable – risk prostate cancer.
48. Timmerman RD. An overview of hypofractionation and introduction to this issue of seminars in radiation oncology. Seminars in radiation oncology. 2008;18(4):215-22.
49. Dasu A, Toma-Dasu I. Dose-effect models for risk-relationship to cell survival parameters. Acta Oncol. 2005;44(8):829-35.
50. Schneider U, Stipper A, Besserer J. Dose-response relationship for lung cancer induction at radiotherapy dose. Z. Med. Phys. 2010;20(3):206-14.

51. Schneider U, Sumila M, Robotka J, Gruber G, Mack A, Besserer J. Dose-response relationship for breast cancer induction at radiotherapy dose. Radiat Oncol. 2011;6(67):1-7.
52. John Ng, Shuryak I. Minimizing second cancer risk following radiotherapy: current perspectives. Cancer management and research. 2015;7:1-11.
53. Schneider U, Besserer J, Mack A. Hypofractionated radiotherapy has the potential for second cancer reduction. Theoretical biology and medical modelling. 2010;7(4):1-6.
54. Liauw SL, Sylvester JE, Morris CG, Blasko JC, Grimm PD. Second malignancies after prostate brachytherapy: incidence of bladder and colorectal cancers in patients with 15 years of potential follow-up. Int J Radiation Oncology Biol Phys. 2006;66(3):669-73.
55. Rowe J, Grainger A, Walton L, Silcocks P, Radatz M, Kemeny A. Risk of malignancy after gamma knife stereotactic radiosurgery. Neurosurgery. 2007;60(1):60-6.
56. Berrington de Gonzalez A, Wong J, Kleinerman R, Kim C, Morton L, Bekelman JE. Risk of second cancers according to radiation therapy technique and modality in prostate cancer survivors. Int J Radiation Oncology Biol Phys. 2015;91(2):295-302.
57. Bicron H. Model 5500 automatic TLD reader user's manual.1993.
58. IAEA Publication. Technical Report Series 457 Dosimetry in diagnostic radiology: An international code of practice.2007.

APPENDIX

1. TLD-700 Calibration [57]

1.1 TLD-700 selection

i. Imperfect TLDs were cut out and residual TLDs were arranged on sachet.

ii. Residual TLDs were activated by irradiation with Co-60 machine which exposed 50 cGy on field size 15 x 15 cm^2 at depth 0.5 cm.

iii. Irradiated TLDs were annealed by heating 400^oC in 1 hour and 100^oC in 2 hours.

iv. TLDs were repeated in process i to iii in 3 times.

1.2 TLD-700 calibration

i. Selected TLDs were put on solid water phantom and exposed by Co-60 machine which prescribed dose 50 cGy on field size 15 x 15 cm^2 at depth 0.5 cm.

ii. Irradiated TLDs were heated by heating 100^oC in 1 hour.

iii. Irradiated TLDs were read signal by TLD reader system and recorded results.

iv. Selected TLDs were repeated in process i to iii in 2 times.

v. Mean value were defined for individual TLDs and all TLDs to calculate element correction coefficient (ECC_i) which calculated by equation below.

$$ECC_i = \frac{\text{Mean value of individual TLD}}{\text{Mean value of all TLD}}$$

vi. The 15 TLDs which there are ECC_i values closed to 1 were selected. These TLDs were standard TLD group that they used for reader calibration factor (RCF) calculation.

vii. The 15 TLDs were defined mean of corrected charge integral $\overline{Q}_{ci}$ which computed by using equation below:

$$\bar{Q}_{ci} = \frac{\Sigma(\text{Mean of individual TLD} \times ECC_i)}{n}$$

Where ECC_i is element correction coefficient of the i-th TLD and n is number of TLDs

RCF calculated by using equation below:

$$RCF = \frac{\overline{Q}_{ci}}{D}$$

Where $\overline{Q}_{ci}$ is mean of corrected charge integral of standard TLD group and D is irradiated dose of 50 cGy.

viii. The 100 TLDs were selected for calibration

ix. The 100 TLDs were repeated in process i to iii in 2 times for determining the individual element correction coefficient (ECC_{ci}) of each TLD which calculated according to the following relationship:

$$ECC_{ci} = \frac{RCF \times D}{Q_i}$$

Where D is irradiated dose of 50 cGy and Q_i is individual charge reading of i-th TLD.

x. Absorbed dose of each TLD were calculated as follows:

$$D_u = \frac{Q_i \times ECC_{ci}}{RCF}$$

Where D_u is unknown absorbed dose and Q_i is individual charge reading of each TLD.

Table A.1 The element correction coefficient (ECC_i) of 100 TLDs.

TLD No.	ECC_i	ECC_{ci}	TLD No.	ECC_i	ECC_{ci}
1	1.00000	1.01294	35	0.97722	0.98065
2	0.99690	1.03579	36	0.98008	1.04174
3	1.00082	0.94888	37	0.98061	1.03168
4	1.00362	0.96211	38	0.98176	1.02017
5	1.00218	0.96282	39	0.98339	1.01552
6	1.00164	0.96386	40	0.97549	1.01582
7	1.00039	1.00015	41	0.98002	0.99663
8	0.99642	0.97671	42	0.97504	1.01275
9	1.00295	1.01124	43	0.97811	0.97422
10	1.00229	0.99205	44	0.98460	0.99191
11	0.99811	0.97950	45	0.98021	1.05273
12	0.99813	0.98708	46	0.97502	0.99267
13	0.99776	0.99973	47	0.99296	1.00845
14	1.00284	0.97712	48	0.99329	1.02493
15	1.00264	0.99292	49	0.99305	1.00478
16	1.00357	0.96547	50	0.98939	0.99910
17	1.00231	1.01796	51	1.01496	1.04444
18	0.97483	0.99899	52	1.01327	1.04546
19	0.96879	1.01993	53	1.01251	1.03064
20	0.96679	0.93172	54	1.00556	1.06887
21	0.97333	0.96036	55	1.00508	1.00589
22	0.96885	0.98217	56	1.00855	1.01429
23	0.96690	1.00006	57	1.01106	1.11981
24	0.97168	0.99714	58	1.02431	1.00225
25	0.97084	0.98382	59	1.01655	1.03921
26	0.97238	0.96585	60	1.02472	1.04025
27	0.96796	0.97283	61	1.01567	1.03044

Table A.1 The element correction coefficient (ECC_i) of 100 TLDs (continued).

TLD No.	ECC_i	ECC_{ci}	TLD No.	ECC_i	ECC_{ci}
28	0.97205	0.95418	62	1.02375	1.04645
29	0.96781	1.00196	63	1.01812	1.03762
30	0.96528	1.00404	64	1.02487	1.07829
31	0.97082	0.93596	65	1.02622	1.05346
32	0.96606	1.05448	66	1.03334	1.03226
33	0.97135	1.00362	67	1.03298	1.15373
34	0.97349	1.01487	68	1.02879	1.05475
69	1.03450	0.95617	85	0.95549	0.96848
70	1.02977	0.96780	86	0.96427	0.97828
71	1.03230	0.98807	87	0.95858	0.94981
72	1.03313	0.95719	88	0.95521	0.95023
73	1.03699	0.93632	89	0.96115	0.92951
74	1.04075	0.96058	90	0.96157	0.95745
75	1.03715	0.96824	91	0.95731	0.94407
76	1.03865	0.97527	92	0.95332	0.97089
77	1.04207	0.92578	93	0.94596	0.95388
78	1.03745	0.92023	94	0.94534	0.98018
79	1.04714	0.93230	95	0.94839	0.93733
80	1.04757	0.95883	96	0.94848	0.97673
81	1.05163	0.94516	97	0.95415	0.94005
82	1.05432	0.96096	98	0.94833	0.92036
83	1.05524	0.97200	99	0.94527	0.93734
84	0.95681	0.97000	100	0.95244	0.97363

1.3 Linearity test for TLD-700

For linearity test of TLD-700, TLDs were irradiated with radiation dose 0.05, 0.10, 0.25, 0.50 and 1.00 Gy. Averaged dose measurement of TLDs was plotted on linear scale as a function of irradiated dose. The linearity of TLD is presented in Figures A1 which is a linear relation with a $R^2 = 0.9999$ (Figure A.1).

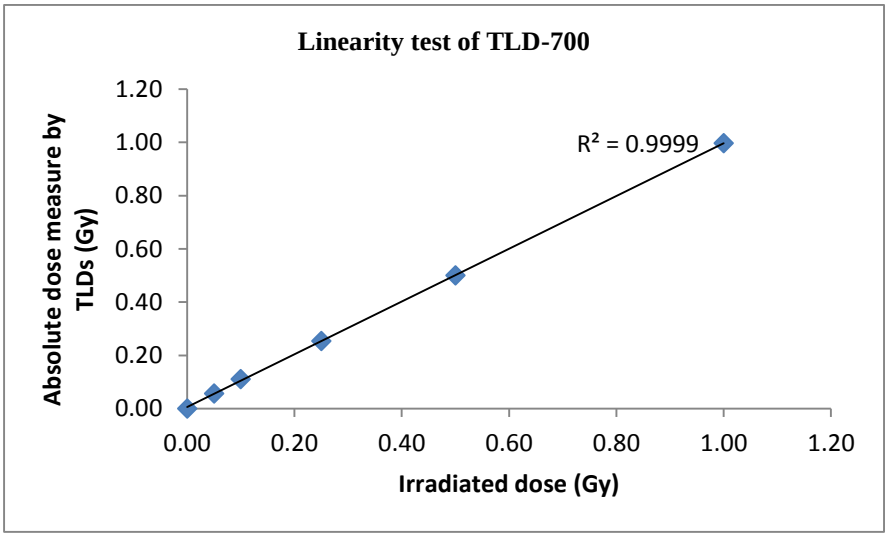

Figure A.1 linearity test for TLD-700.

2. TLD-100H Calibration [58]

2.1 TLD-100H preparation

i. Imperfect TLDs were removed from the group.

ii. Three TLDs were set to measure background signal.

iii. Residual TLDs were activated by using kilo-voltage x-ray beam which open field size 10 x 10 cm^2 at SSD 100 cm, 105 kV, 400 mA and 200ms.

iv. Irradiated TLDs were annealed by heating 240^oC in 10 minutes.

v. TLDs were repeated in process iii to iv for 5 times.

2.2 TLD-100H selection

i. All residual TLDs were arranged on the sachet and place them on the Styrofoam at irradiation position which used field size 10 x 10 cm^2 at SSD 100 cm (reference position).

ii. The TLDs were exposed x-ray energy 105 kV, 400 mA and 200 ms (≈ 8mGy) by using x-ray kV source of On Board Imaging system which mounted on Linac machine. Three TLDs for background measurement were unexposed x-ray.

iii. Irradiated TLDs (M_1, M_2,…., M_n) and three TLDs (M_{01}, M_{02} and M_{03}) for background measurement were read signal by TLD reader system and record results

iv. Mean value of background signal from three TLDs ($\overline{M}_0$) were calculated as following:

$$\overline{M}_0 = \frac{M_{01} + M_{02} + M_{03}}{3}$$

v. Mean value of exposed signal ($\overline{M}$) and standard deviation (SD) were calculated from each exposed TLDs signal which eliminated mean value of background by equation below:

$$\overline{M} = \frac{\sum_{i=1}^{n} M_i - \overline{M}_0}{n}$$

$$SD = \sqrt{\frac{(\sum_{i=1}^{n} M_i - \overline{M})^2}{n-1}}$$

Where M_i is average individual charge reading of i-th TLD and n is number of TLDs.

vi. The TLDs were selected when exposed TLDs signal, eliminated mean background signal ($M_i - \overline{M}_0$), within the interval ($\overline{M} \pm 3SD$).

vii. The signal of remaining TLDs were calculated for individual sensitivity factor (k_{si}) by equation below:

$$k_{si} = \frac{\overline{M}}{M_i - \overline{M}_0}$$

Where M_i is average individual charge reading of i-th TLD and $\overline{M}_0$ is mean value of background signal.

2.3 TLD-100H calibration

i. Reference dosimeter (Radcal 6 cc ionization chamber) were set at reference position which open field size 10 x 10 cm^2 at SSD 100 cm on Styrofoam and placed the isocenter of beam on the center of ionization chamber.

ii. Exposure values (mR) were measured by using x-ray source of Linac machine. X-ray parameter was 105 kV, 400mA and 200ms (8 mGy). Mean of exposure values (M_Q^{ref}) were defied from ionization chamber measurement in 10 times.

iii. All TLD-100H exclude three background TLDs were exposed kV x-ray at reference position and used the same x-ray parameter as reference dosimeter.

iv. Mean value of background signal from three TLDs ($\overline{M}_0$) were calculated as following:

$$\overline{M}_0 = \frac{M_{01} + M_{02} + M_{03}}{3}$$

v. Mean of exposed TLD ($\overline{M}_Q$) that each TLD were corrected individual sensitivity factor were calculated as following:

$$\overline{M}_Q = \frac{\sum_{i=1}^{n} k_{si}\left(M_i - \overline{M}_0\right)}{n}$$

Where M_i is average individual charge reading of i-th TLD and $\overline{M}_0$ is mean value of background signal. n is number of TLDs.

vi. The calibration coefficient ($N_{k,Q}$) of TLDs were calculated from by equation below:

$$N_{k,Q} = \frac{M_Q^{ref}}{M_Q} \cdot N_{k,Q_0}^{ref} \cdot k_{Q_{cross}}^{ref}$$

Where N_{k,Q_0}^{ref} is the calibration coefficient of ionization chamber which obtained from manufacturer and $k_{Q_{cross}}^{ref}$ is the beam quality correction ($k_{Q_{cross}}^{ref}$ = 1).

vii. Unknown dose (D_u) were calculated as following:

$$D_u = \overline{M}_Q \times N_{k,Q} \times R \times B_s \times \mu$$

Where R is exporsure to Gy conversion factor (R = 0.00876 mGy/mR), B_s is backscatter factor and μ is attenuation factor.

Table A.2 The individual sensitivity factor (k_{si}) of TLD-100H.

TLDs No.	k_{si}	TLDs No.	k_{si}
1	1.39802	26	1.02016
2	1.18084	27	1.13700
3	1.32182	28	0.92593
4	1.28352	29	0.89499
5	1.39080	30	0.94984
6	1.20268	31	1.07763
7	1.05490	32	1.26917
8	1.00399	33	1.24542
9	1.14091	34	1.16927
10	1.40298	35	0.92641
11	1.15044	36	1.14790
12	1.21574	37	1.23008
13	1.29995	38	1.15199
14	1.46146	39	1.23136
15	1.13063	40	1.16031
16	1.15540	41	1.20491
17	1.02016	42	1.35731
18	1.26932	43	1.30450
19	1.40877	44	1.07795
20	1.35523	45	0.99196
21	1.03787	46	0.94390
22	0.96006	47	0.92229
23	1.11449	48	0.85630
24	1.04577	49	0.95333
25	1.25190	50	1.08846

Table A.2 The individual sensitivity factor (k_{si}) of 100 TLDs (continued).

TLDs No.	k_{si}	TLDs No.	k_{si}
51	1.00677	76	0.75362
52	1.00614	77	1.00966
53	1.08818	78	1.03185
54	1.19385	79	0.92858
55	1.09820	80	0.93317
56	0.91553	81	1.00249
57	1.01356	82	1.04683
58	1.03214	83	0.77329
59	1.02521	84	0.79298
60	0.78859	85	0.81330
61	1.00224	86	1.18730
62	0.96766	87	0.97180
63	0.99352	88	0.94656
64	0.92249	89	1.06182
65	1.01709	90	0.88022
66	0.72970	91	1.01258
67	0.97571	92	1.03129
68	1.00687	93	0.98050
69	0.88772	94	0.83371
70	0.77181	95	0.82223
71	0.95279	96	0.83679
72	0.99170	97	1.02950
73	0.75797	98	0.89921
74	0.75701	99	0.83139
75	0.69298	100	0.99982

2.4 Linearity test for TLD-100H

For linearity test of TLD-100H, TLDs were irradiated with 0.5, 1, 16, 40, 64, 80, 100 and 126 mAs. Averaged signal reading of TLDs was plotted on linear scale as a function of mAs. The linearity of TLD is presented in Figures A2 which is a linear relation with a $R^2 = 0.9764$ (Figure A.2).

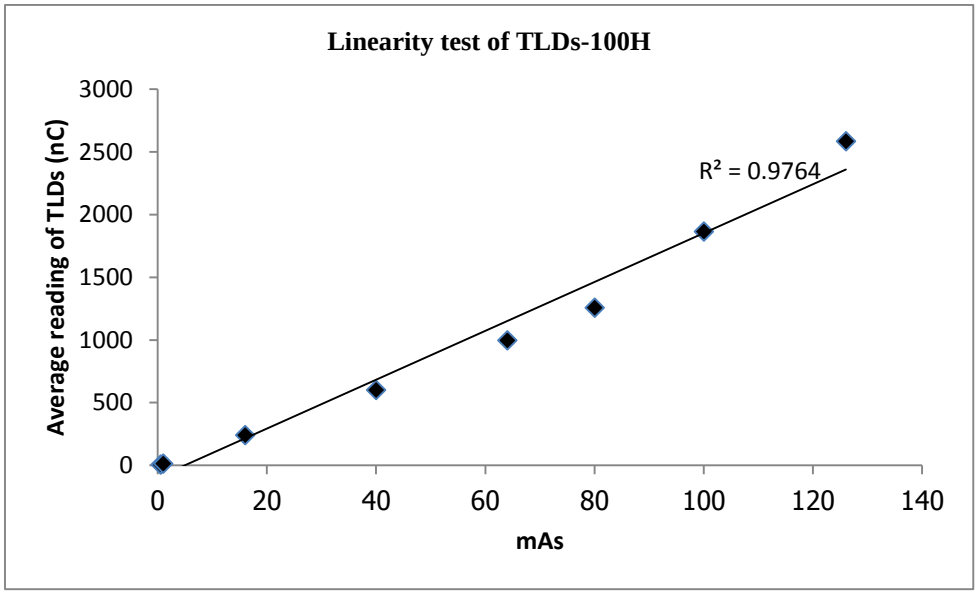

Figure A.2 linearity test for TLD-100H.

BIOGRAPHY

NAME	Miss Sawanee Suntiwong
DATE OF BIRTH	29 June 1985
PLACE OF BIRTH	Nakhornratchasima, Thailand
INSTITUTIONS ATTENDED	Mahidol University, 2005: Bachelor of Science (Radiological Technology) Mahidol University, 2014: Master of Science (Medical Physics)
OFFICE	Chulabhorn Hospital, 54 Kamphaeng Phet 6, Talat Bang Khen, Laksi, Bangkok, Thailand 10210 Tel. 0-2576-6038
HOME ADDRESS	307 Chainorong Road, Muang, Nakhonratchasima, Thailand 30000 Tel. 0-4426-5118